



# Mercury dynamics in a changing coastal area over industrial and postindustrial phases: Lessons from the Venice Lagoon

Ginevra Rosati\*, Cosimo Solidoro, Donata Canu

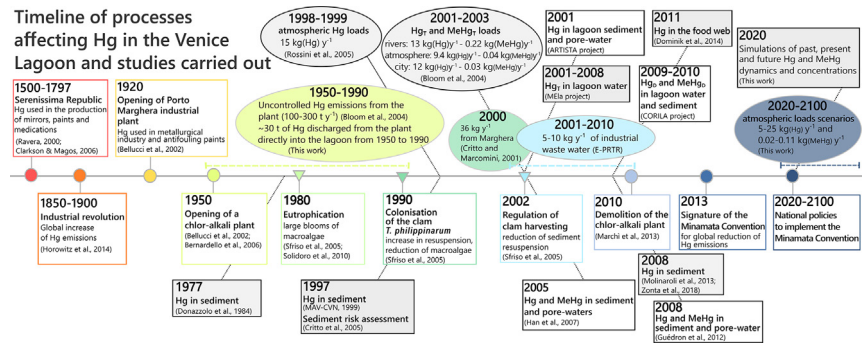
National Institute of Oceanography and Applied Geophysics - OGS, Trieste, Italy



## HIGHLIGHTS

- The Venice Lagoon was subjected to high Hg loadings during the industrial time.
- A spatially explicit model was used to reconstruct the temporal evolution of Hg.
- The model for Hg in water and sediment was integrated with available data.
- Impacts of eutrophication and sediment resuspension on Hg fluxes were explored.
- This allowed for reconstruction of historical dynamics using a holistic approach.

## GRAPHICAL ABSTRACT



## ARTICLE INFO

### Article history:

Received 5 March 2020

Received in revised form 25 June 2020

Accepted 26 June 2020

Available online 02 July 2020

Editor: Mae Sexauer Gustin

## ABSTRACT

During the industrial period, significant amounts of mercury (Hg) were discharged into the Venice Lagoon. Here, a spatially explicit model was implemented to reconstruct the temporal evolution of the total mercury ( $Hg_T$ ) and methylmercury ( $MeHg_T$ ) concentrations in lagoon water and sediments over two centuries (1900–2100), from preindustrial to postindustrial phases. The model simulates the transport and transformations of particulate and dissolved Hg species. It is forced with time-variable Hg inputs and environmental conditions, including scenarios of future atmospheric deposition, reconstructed according to local and global socioeconomic scenarios. Since 1900, ~36 Mg of  $Hg_T$  and ~380 kg of  $MeHg_T$  were delivered to the lagoon, and stored in the sediments. The deposition of Hg from the water to the seafloor increased during a period of eutrophication (1980s); however, the reverse fluxes increased during a period of high sediment resuspension caused by the unregulated fishing of Manila clams (1990s). In the current postindustrial phase, the lagoon sediments have acted as a secondary source to the lagoon waters, delivering Hg (~38 kg y<sup>-1</sup>) and MeHg (~0.07 kg y<sup>-1</sup>). The MeHg inputs from the watershed (~0.28 kg y<sup>-1</sup>) appear to be higher than the secondary fluxes from the sediments. The estimated  $Hg_T$  export to the Adriatic Sea is ~56 kg y<sup>-1</sup>. Since  $Hg_T$  and  $MeHg_T$  outputs slightly exceed inputs, the concentrations are slowly decreasing. While the decreasing trend is maintained in all scenarios, the future level of atmospheric deposition will affect Hg concentrations and sediment recovery times. Though limited by inherent simplifications, this work results show that the reconstruction of historical dynamics using a holistic approach, supported by data, can improve our understanding of the pollutants distribution and the quantification of local emissions. Downscaling from trends predicted at the global scale taking into account for regional differences seems useful to investigate the pollutants fate.

© 2020 Elsevier B.V. All rights reserved.

\* Corresponding author.  
E-mail address: [grosati@inogs.it](mailto:grosati@inogs.it) (G. Rosati).

## 1. Introduction

In most Western countries, society is in a postindustrial phase, and coastal sites are currently exposed to pollutant loads that are much lower than those of the past (Amos et al., 2015; Turner et al., 2018); in fact, values may be similar to preindustrial levels. However, because some of these sites have been exposed to higher direct contamination for decades, it is useful and interesting, though challenging, to reconstruct the long-term dynamics of persistent pollutants to better assess and understand the present situation and to frame it in a larger perspective. This manuscript focuses on the biogeochemical cycle of a persistent pollutant of global concern (mercury, Hg) in a very well-studied site (the Venice Lagoon, Italy) that has gone through an important industrial phase.

Hg in water and sediment undergoes biological and photochemical reactions (Black et al., 2012; Fitzgerald, 2006; Heyes et al., 2006; Hines et al., 2012; Hollweg et al., 2009; Lehnher et al., 2011; Monperrus et al., 2007a, 2007b; Qureshi et al., 2010; Sharif et al., 2014) that result in the net production, bioaccumulation and biomagnification of neurotoxic monomethylmercury (MMHg) in marine food webs at a global scale (Cossa et al., 2012; Schartup et al., 2019; Storelli and Barone, 2013). The direct input of Hg to the environment is currently banned in most countries, and the amount of Hg that is released from anthropogenic land-based activities and enters marine ecosystems is relatively small; these inputs are from uncontrolled wastewater discharge, water run-off, and atmospheric deposition. Land-originated inputs of methylated Hg species (MeHg, as the sum of MMHg and dimethylmercury, DMHg) are a small fraction of the total mercury ( $Hg_T$ ) and are usually low compared to in situ production (Bloom et al., 2004; Mason et al., 2012). Nonetheless, a large variability exists, and only local assessments can reveal the relative importance of external versus in situ MeHg sources across ecosystems (Balcom et al., 2015; Cossa et al., 2017; Melaku Canu et al., 2015; Rosati et al., 2018; Schartup et al., 2015a).

A number of ecosystems that received substantial Hg inputs from primary emissions during the past industrial period are now enriched in Hg, acting as secondary Hg sources and possibly serving as secondary sources for long periods (Canu and Rosati, 2017; Kocman et al., 2013; Rudd et al., 2018; Salvagio Manta et al., 2016). Re-emission of formerly deposited Hg from coastal sites occur through the reduction of  $Hg^{II}$  and MeHg to  $Hg^0$ , which then evades to the atmosphere, or through mobilization and transport to the open sea of particulate and dissolved Hg species. Globally, the re-emission of anthropogenic Hg from waters and soils has been estimated to contribute to ~60% of the current atmospheric deposition, but this percentage will increase in the near future in the absence of conspicuous emissions reductions (Amos et al., 2013; Sunderland and Selin, 2013). Hg that previously accumulated in an ecosystem, often buried in sediments (Emili et al., 2012; Han et al., 2007; Matteucci et al., 2005; Muresan et al., 2007; Salvagio Manta et al., 2016), can be mobilized and/or lead to substantial MeHg production and bioaccumulation depending on water and sediment transport (Melaku Canu et al., 2015; Rajar et al., 2000; Rudd et al., 2018; Žagar et al., 2006) and biogeochemical conditions (Bravo et al., 2017; Gilmour et al., 2018; Han et al., 2007; Kim et al., 2011; Schartup et al., 2015b; Soerensen et al., 2017; Sunderland et al., 2006). Quantifying secondary fluxes of anthropogenic Hg is extremely important for policymakers; however, fluxes from contaminated terrestrial sites to the hydrosphere and fluxes from coastal areas to the open sea are poorly characterized (Kocman et al., 2013; Selin et al., 2018). As stated by the Minamata Convention (Selin et al., 2018), it is important to develop methods to integrate data into an evaluation framework and improve Hg modeling tools and methods to anticipate local and global effects of Hg emissions reduction efforts (Amos et al., 2013; Canu and Rosati, 2017; Chen et al., 2018; Kocman et al., 2013; Sunderland and Selin, 2013) as well as alterations to the Hg cycle related to climate change (Alava et al., 2017; Canu and Rosati, 2017; Schartup et al., 2019).

In this paper, a numerical biogeochemical model for three Hg species (inorganic mercury,  $Hg^{II}$ , elemental mercury,  $Hg^0$ , and methylmercury, MeHg) (Section 2.4) is used in a spatially explicit configuration to explore the time course (1900–2100) of Hg and MeHg concentrations and dynamics in a Mediterranean lagoon (the Venice Lagoon) under changing environmental conditions (Section 2.5) and Hg inputs that are representative of the preindustrial, industrial and postindustrial phases (Section 2.3). In fact, the Venice Lagoon (Section 2.1) received inputs from a chlor-alkali plant and other industrial activities from the 1930s to the early 2000s (Bernardello et al., 2006) and faced other environmental challenges due to high anthropic pressures, such as eutrophication and sediment loss (Sarretta et al., 2010; Sfriso et al., 2005; Melaku Canu et al., 2011; Solidoro et al., 2010). The model was used to verify whether or not the role of the Venice Lagoon sediment as a sink or source for anthropogenic Hg has changed over time as a result of the interactions among these processes, and if yes to what extent. The model has already been applied to Hg cycling in other marine ecosystems (Melaku Canu et al., 2015; Canu and Rosati, 2017; Rosati et al., 2018), and here, it is forced with time-variable Hg inputs estimated in this work (Sections 2.3 and 3.1) according to the evolution of socioeconomic activities and technologies, including future scenarios (Section 2.5) of atmospheric deposition (Chen et al., 2018). The model results are constrained with field data (Section 3.2) on Hg species in sediment, water and pore water available from previous assessments that have been carried out since 1977 during different research projects (Section 2.2). The budget for  $Hg_T$  and MeHg<sub>T</sub> in the present state (2019) (Section 3.4) and the recovery time for sediment to reach Hg concentrations that are in compliance with Italian law ( $0.3 \mu g g^{-1}$ ) are estimated (Section 3.5), and the modeled impacts of past environmental changes on Hg species dynamics are discussed (Section 3.3).

## 2. Methods

The site and its present and historical Hg contamination levels are presented in Section 2.1; the dataset used to compare the model results is presented in Section 2.2. The methods used to quantify the  $Hg_T$  and MeHg<sub>T</sub> inputs from natural and anthropogenic sources are presented in Section 2.3. The model structure and the model implementation for the Venice Lagoon are presented in Sections 2.4 and 2.5, respectively.

### 2.1. Study site: historical setting and present conditions

The Venice Lagoon (northern Adriatic Sea, Italy) is a shallow coastal lagoon (Fig. 1) with a surface area of approximately 550 km<sup>2</sup>. The lagoon receives freshwater inflows ( $\sim 1.1 \cdot 10^9 m^3 y^{-1}$ ) from 12 main tributaries (Zuliani et al., 2005) and is connected to the Adriatic Sea through three inlets (Lido, Malamocco and Chioggia inlets). The city of Venice is located in the northern-central sector of the lagoon, and the urbanization of Venice dates back to the XIII century when the 'Serenissima Republic of Venice' was an important player in international trades. Legislation to protect human health and the environment was adopted as early as the XV century, when some industries were moved to neighboring islands (Ravera, 2000). In the 1920s, metallurgical industries were settled on the mainland in 'Porto Marghera', and the site was later expanded with the addition of chemical and petrochemical factories, including a chlor-alkali plant that became active in 1951 (Solidoro et al., 2010). Industries and infrastructures account for 21% of the watershed surface area ( $\sim 1880 km^2$ ), cultivated areas account for 66%, other green areas account for 6%, and urban and residential areas account for 7% (Bendoricchio et al., 1993). The 1980s were characterized by massive eutrophication phenomena (Solidoro et al., 1997a, 1997b), while the 1990s were characterized by disruptive sediment perturbation related to uncontrolled clam fishing (Solidoro et al., 2000; Pastres et al., 2011). Currently, Venice is a popular tourist destination with a sharply decreasing population (from 184,000 inhabitants in 1950 to 70,000 inhabitants in the 2000s), and there has been a decline in

## The Venice Lagoon

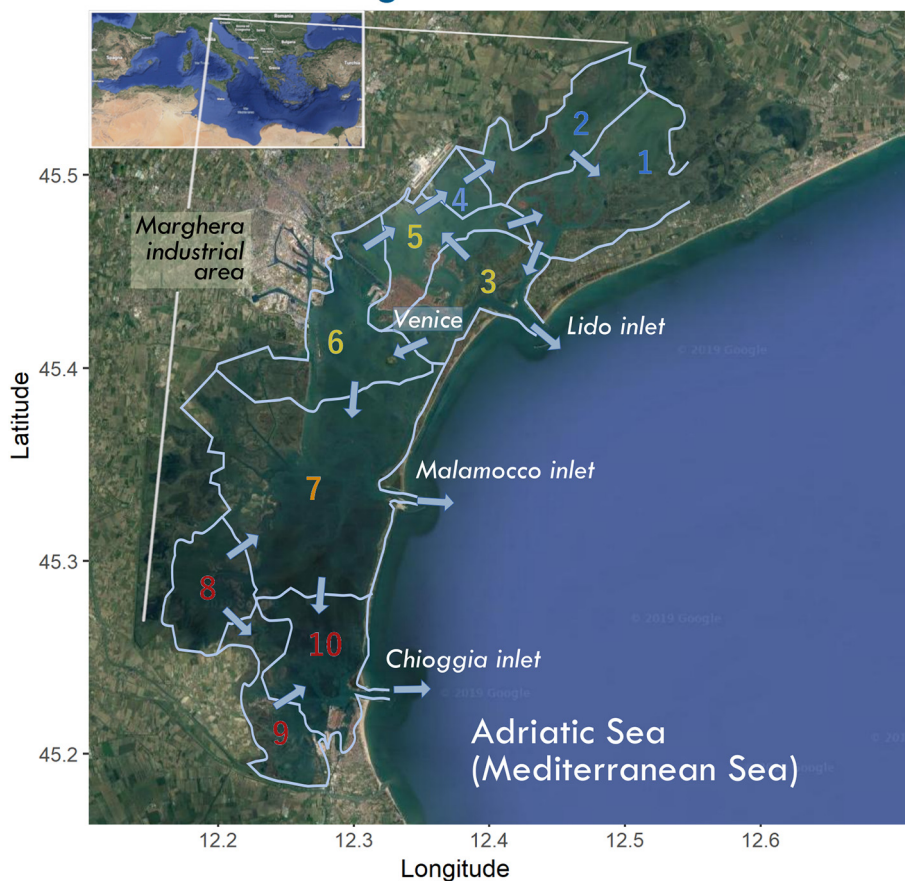


**Fig. 1.** Map of the Venice Lagoon with contours and numbers of the 10 sub-basins used for model partitioning into boxes. The sub-basins are identified based on hydrodynamic properties (Solidoro et al., 2004); sub-basins 1, 2 and 4 are in the northern lagoon, sub-basins 3, 5, 6, and 7 are in the central lagoon and sub-basins 8, 9 and 10 are in the southern lagoon. The location of the city of Venice and the industrial area of Porto Marghera are shown.

industrial activities in the area as well as general technological improvement in terms of emissions control in Western countries (Streets et al., 2017, 2011).

Since the late 1970s, several studies and monitoring projects have been carried out to assess the Hg concentrations in the lagoon sediment, water, and food webs. Fig. S1 summarizes the anthropogenic activities that most impacted the Hg cycle in the Venice Lagoon during different periods, along with studies and environmental monitoring programs that have addressed the presence of mercury in the area (Bellucci et al., 2002; Bettiol et al., 2005; Bloom et al., 2004; Critto et al., 2005; Critto and Marcomini, 2001; Dominik et al., 2014; Donazzolo et al., 1984; Guédron et al., 2012; Guerzoni and Tagliapietra, 2006; Han et al., 2007; Kim et al., 2011; MAV-CORILA, 2011; MAV-CVN, 2005, 2004, 1999; Molinaroli et al., 2013; Pavoni et al., 1987; Rossini et al., 2005; Zonta et al., 2018).

Currently, it appears that the  $Hg_T$  concentrations in the surface sediment ( $0.03\text{--}2.3\ \mu\text{g g}^{-1}$ , Table S1) of the Venice Lagoon have the potential to have adverse biological effects, exceeding both the ecotoxicological thresholds the “Effect Range-Low” (ERL =  $0.15\ \mu\text{g g}^{-1}$ ) in 86% of the lagoon area and the “Effect Range-Median” (ERM =  $0.71\ \mu\text{g g}^{-1}$ ) in 20% of the lagoon area (Critto et al., 2005; Zonta et al., 2018) and the limit of  $0.3\ \mu\text{g g}^{-1}$  set by Italian legislation (Ministerial Decree n. 260 28/11/2010) under the EU Water Framework Directive (WFD, 2000/60/EC). A basin-wide assessment carried out in 2002 (Bloom et al., 2004) found unfiltered water concentrations ranging from  $2\text{--}100\ \text{ng l}^{-1}$  for  $Hg_T$  to  $36\text{--}327\ \text{pg l}^{-1}$  for  $MeHg_T$  (Table S1); additionally, dissolved Hg and MeHg ( $Hg_D$  and  $MeHg_D$ ) concentrations in filtered water ranging from  $2.6\text{--}4.7\ \text{ng l}^{-1}$  and  $104\text{--}293\ \text{pg l}^{-1}$ ,

respectively, were measured in the central lagoon during 2009–2010 (MAV-CORILA, 2011, Table S1). The  $Hg_T$  concentrations measured in edible fish species (Dominik et al., 2014) are below the threshold for Hg in seafood ( $0.5\ \mu\text{g g}^{-1}$  wet weight) set by the EU.

### 2.2. Mercury species data and ancillary data

A database of measured Hg and MeHg concentrations in sediment, pore water and water (Table S1), spanning the 1970–2010, was constructed to evaluate and corroborate model results by merging all the available information (Bloom et al., 2004; Donazzolo et al., 1984; Guédron et al., 2012; Guerzoni and Tagliapietra, 2006; Han et al., 2007; Kim et al., 2011; MAV-CORILA, 2011; MAV-CVN, 2005, 2004, 1999; Zonta et al., 2018) from published papers and reports produced by local institutions, such as the “Magistrato alle Acque di Venezia (MAV)”, the “Consortium for coordination of research activities concerning the Venice Lagoon system (CORILA)”, and the “Regional Agency for Environmental Protection and Prevention of the Veneto” (ARPAV).

Other ancillary data were gathered to force the model environmental dynamics (Section 2.4), namely, water temperature (2001–2005) (MAV-CVN, 2004; 2005), sunlight irradiance (2010–2019) (ARPAV, <http://www.arpa.veneto.it>), water fluxes (Solidoro et al., 2004; Zuliani et al., 2005) and river sediment load ( $\sim 33,400\ \text{t y}^{-1}$ ) (Collavini et al., 2005). Monthly concentrations of suspended particulate matter (SPM) and particulate organic matter (POM) for 2001–2005 (MAV-CVN, 2004; 2005) were used to compare the modeled and observed

concentrations and calibrate the sediment resuspension processes in the corresponding period (Section 2.5).

### 2.3. Estimates of historical evolution and future scenarios of mercury emissions and inputs to the lagoon

The time evolution of  $Hg_T$  and  $MeHg_T$  inputs to the lagoon from each source (rivers, atmosphere, industries, and urban wastes) was estimated to force the evolution of the  $Hg_T$  and  $MeHg_T$  concentrations in the model. To do so, existing data and estimates for the area were considered (Bloom et al., 2004; EEA, European Pollutant Release and Transfer Register, n.d.; Rossini et al., 2005), as was the evolution of local and global anthropogenic drivers affecting Hg emissions and loadings. Downscaling from global modeling was performed to reconstruct the historical course of river input (Amos et al., 2014), atmospheric deposition of Hg (Amos et al., 2015), and industrial load (Streets et al., 2017, 2011), as well as the possible scenarios of the future atmospheric deposition rates (Chen et al., 2018).

In the Venice industrial area of Porto Marghera, two industrial facilities have been particularly relevant concerning Hg emissions: a zinc smelting plant and a chlor-alkali plant that have been active since 1936 and 1951, respectively. The industrial emissions related to these sources were estimated by combining the time-variable production rates for each facility (ARPAV, 2007; Marchi et al., 2013; Ministero dell'Ambiente e della Tutela del Territorio e del Mare, 2007; Perugini, 2014; Porchia, 2012) and the Hg emission factors to air and water (Berdowski et al., 2017; Brinkmann et al., 2014; Joint Research Center of the European Commission, 2001; Streets et al., 2017, 2011; Turner et al., 2018) for each process considered, as explained in more detail in Text S1, Table S2 and Fig. S2. Since very high Hg concentrations (up to  $20 \mu\text{g g}^{-1}$ ) were measured in the sediments of the industrial channels (Bellucci et al., 2002), it was assumed that 30% of the estimated Hg emissions to the water were deposited in those channels (Text S1) and that the remaining emissions were delivered to the lagoon toward box 6. This assumption is based on the global estimates of Hg stored at contaminated sites (~40% in Streets et al., 2017) and was further adjusted to fit the estimated amount of Hg released to the lagoon water with the release data reported from industrial facilities for 1998–2006 (EEA, European Pollutant Release and Transfer Register) (Text S1 and Fig. S2E).

For the period before industrialization in the Venice area (1900–1930), the river Hg load to the lagoon ( $6.8 \text{ kg y}^{-1}$ ) was estimated based on the background Hg concentrations in the soils of the watershed (Molinarioli et al., 2013) and sediment load (Collavini et al., 2005). The time evolution of the river Hg load was estimated by scaling the load in 2002 ( $13.2 \text{ kg y}^{-1}$ ) (Bloom et al., 2004) according to the enrichment factors for Hg in European rivers (Fig. S3a), as calculated by Amos et al. (2014). The  $MeHg$  inputs were set throughout the simulation to be 1.7% of  $Hg_T$  for rivers and 1% of  $Hg_T$  for industrial inputs, which agrees with previous observations for the study area (Bloom et al., 2004).

Both river and industrial loads were assumed to decrease linearly ( $-1.5\% \text{ y}^{-1}$ ) since 2002 and 2010, respectively, due to progressive regulatory improvements in Europe concerning environmental regulations, wastewater treatment and Hg use in commercial products (Amos et al., 2014; Horowitz et al., 2014; Marnane et al., 2018; Streets et al., 2019). For the industrial load, the trend was projected to the end of the simulations (2100), assuming a decreasing amount of Hg would be continuously transferred from the industrial channels to the lagoon water through navigation and tidal flushing for many years after the closure of the chlor-alkali plant. For the river load, the decline ends when the preindustrial levels are reached that occurs in 2050.

The time evolution of Hg atmospheric deposition was estimated by scaling the observed value for 1999 ( $\sim 12 \text{ kg y}^{-1}$ ) (Rossini et al., 2005) according to the enrichment factors estimated for global Hg atmospheric deposition (Amos et al., 2015), maintaining the Hg atmospheric

deposition rate within the range predicted for marine areas (Fig. S3b) from an ensemble of global models (AMAP/UNEP, 2013). The observed decreasing trend of Hg atmospheric deposition in Europe ( $-1.5\% \text{ y}^{-1}$  from 1990 to 2012) (Colette et al., 2016) was used to scale the Hg atmospheric inputs from 1999 to 2015. After 2015, five scenarios were considered: the value of atmospheric deposition was maintained as constant in the Reference simulation, and four alternative possibilities were explored for the period of 2015–2100 (Fig. S3b) based on global model projections for 2015–2050 (Chen et al., 2018), which are extended here until 2100. The “Zero Emissions (ZE)” scenario simulates a rapid decline in the atmospheric deposition rate from 2015 to 2020 and a slower decrease after 2020. The “Emission Control (EC)” scenario assumes a 50% decline in Hg emissions and simulates a less marked decrease in atmospheric deposition than that in the “ZE” scenario. The “Constant Emissions (B1)” scenario assumes constant primary Hg emissions and increasing atmospheric deposition, while the “Business-as-Usual (A1B)” scenario simulates rapid economic growth and continuous emissions growth, resulting in the highest increase in atmospheric deposition.

A further source of Hg to the lagoon is the network of navigable channels in Venice city (Bloom et al., 2004); these sources are likely caused by ship-induced resuspension of sediments that have accumulated Hg over time and recent inputs from urban sources. This input was assumed to be  $3 \text{ kg y}^{-1}$  at the beginning of the simulation, and the value increased to  $12 \text{ kg y}^{-1}$  in 2001 that is in agreement with the measurements carried out by Bloom et al. (2004); after 2005, the input decreased based on the progressive decline in Hg use in commercial products in developed countries (Horowitz et al., 2014) and the declining urban population in Venice (Ravera, 2000).  $MeHg_T$  fluxes to the lagoon from the atmosphere and the city channels were considered to be 0.42% and 0.25% of the  $Hg_T$  fluxes, respectively, throughout the simulation, and these values were based on the measurements by Bloom et al. (2004).

### 2.4. The Hg model

The WASP Hg model/MERC7 (Wool et al., 2001) is a deterministic model designed to simulate the cycle of Hg species in aquatic environments (Fig. S4). The model has already been implemented in a 2D framework to simulate the Hg dynamics in the Marano-Grado Lagoon, a shallow lagoon in the northern Adriatic Sea (Canu and Rosati, 2017; Melaku Canu et al., 2015), and in a 1D framework for the Black Sea (Rosati et al., 2018).

The model describes the dynamic evolution of three mercury species ( $Hg^{II}$ ,  $Hg^0$ ,  $MeHg$ ) in their particulate and dissolved phases (Tables S3 and S4, Fig. S4) in water and sediment boxes, as well as the evolution of silt and particulate organic matter (POM). The modeled sediment dynamics (Table S5) are driven by loadings from the watershed, resuspension and deposition velocities, and production and degradation of POM (Tables S5 and S6).

Atmospheric deposition, rivers, and anthropogenic activities add  $Hg_T$  and  $MeHg_T$  to the system (Table S4, Fig. S4), and they are transported between adjoining water boxes and outside of the system marine boundaries at the lagoon inlets based on prescribed fluxes of water advection and dispersion coefficients.  $Hg_{(g)}^0$  volatilizes to the atmosphere due to forcings of current velocity and temperature (Table S4). The partitioning of Hg and  $MeHg$  in dissolved and particulate phases in both water and sediment is described through partition coefficients (Table S3, Eqs. (1)–(4)). Exchanges between water and sediment (Table S4, Fig. S3) involve the settling and resuspension of particulate Hg and  $MeHg$  ( $Hg_P$  and  $MeHg_P$ ) driven by the sediment dynamics (Table S5), as well as the diffusive fluxes of dissolved Hg and  $MeHg$  ( $Hg_D$  and  $MeHg_D$ ) modeled through diffusion coefficients. The net deposition of  $Hg_P$  and  $MeHg_P$  to the seabed results in their burial into deep sediment layers. Modeled transformations (Table S4, Fig. S4), which here are assumed to involve only the dissolved Hg

species, include biological Hg methylation and MeHg demethylation in water and sediment pore water and photochemical reactions (photoreduction, photo-oxidation and photodemethylation) in the water column. Biological Hg methylation is parameterized to increase with temperature, and photochemical transformations are adjusted to light intensity.

In summary, the model considers the processes of transformation among different Hg species, as well as the fluxes related to particulate sedimentation and resuspension and the partitioning of Hg compounds among dissolved, particulate, and bound DOC species in water and sediments. Assuming that partitioning of  $Hg^{II}$  and MeHg in water and sediment boxes is much faster than other processes, it can be considered to occur at thermodynamic equilibrium and is parameterized by means of fractions of a given species with respect to its total ( $f_{Hg-POM}, f_{Hg-silt}, f_{Hg-DOC}, f_{HgCl}, f_{MeHg-POM}, f_{MeHg-silt}, f_{MeHg-DOC}, f_{MeHgCl}$ ) which can be computed from the chemical repartition constants as shown in Eqs. (1)–(4) for  $Hg^{II}$ :

$$f_{Hg_{POM}} = Hg_{POM}/Hg_{tot}^{II} = \frac{POM K_D Hg-POM}{\phi + DOC K_D Hg-DOC + POM K_D Hg-POM + SILT K_D Hg-SILT} \quad (1)$$

$$f_{Hg_{silt}} = Hg_{silt}/Hg_{tot}^{II} = \frac{SILT K_D Hg-silt}{\phi + DOC K_D Hg-DOC + POM K_D Hg-POM + SILT K_D Hg-SILT} \quad (2)$$

$$f_{Hg_{DOC}} = Hg_{DOC}/Hg_{tot}^{II} = \frac{DOC K_D Hg-DOC}{\phi + DOC K_D Hg-DOC + POM K_D Hg-POM + SILT K_D Hg-SILT} \quad (3)$$

$$f_{HgCl_n} = HgCl_n/Hg_{tot}^{II} = \frac{\phi}{\phi + DOC K_D Hg-DOC + POM K_D Hg-POM + SILT K_D Hg-SILT} \quad (4)$$

Consequently, the model equations for Hg species in water (Eqs. (5)–(7)) and sediment (Eqs. (8)–(9)) boxes are as follows:

$$\begin{aligned} \frac{d}{dt} Hg_w^{II} = & -k_{met}^w Q_{10} Hg_w^{II} \{f_{Hg_{DOC}}^w + f_{HgCl_n}^w\} + k_{demet}^w MeHg_w \{f_{MeHg_{DOC}} + f_{MeHgCl}\} \\ & + k_{ph_{oxy}} L_N \{Hg_w^0\} - k_{ph_{red}} L_N Hg_w^{II} \{f_{Hg_{DOC}}^w + f_{HgCl_n}^w\} \\ & - Hg_w^{II} \{v_{s-POM} f_{Hg_{POM}} + v_{s-silt} f_{Hg_{silt}}\} + Hg_{sed}^{II} \{v_{r-POM} f_{Hg_{POM}} + v_{r-silt} f_{Hg_{silt}}\} \\ & - \frac{D_m \phi_{sed}}{z_{sed} / \phi_{sed}} \left\{ \frac{Hg_w^{II} \{f_{Hg_{DOC}}^w + f_{HgCl_n}^w\}}{\phi_w} - \frac{Hg_{sed}^{II} \{f_{Hg_{DOC}}^{sed} + f_{HgCl_n}^{sed}\}}{\phi_{sed}} \right\} \quad (5) \end{aligned}$$

$$\begin{aligned} \frac{d}{dt} MeHg_w = & k_{met}^w Q_{10} Hg_w^{II} \{f_{Hg_{DOC}}^w + f_{HgCl_n}^w\} - k_{demet}^w MeHg_w \{f_{MeHg_{DOC}}^w + f_{MeHgCl}^w\} \\ & - k_{ph_{dem}} L_N MeHg_w \{f_{MeHg_{DOC}}^w + f_{MeHgCl}^w\} \\ & - MeHg_w \{v_{s-POM} f_{MeHg_{POM}}^w + v_{s-silt} f_{MeHg_{silt}}^w\} \\ & + MeHg_{sed} \{v_{r-POM} f_{MeHg_{POM}}^{sed} + v_{r-silt} f_{MeHg_{silt}}^{sed}\} - \frac{D_m \phi_{sed}}{z_{sed} / \phi_{sed}} \\ & \left\{ \frac{MeHg_w \{f_{MeHg_{DOC}}^w + f_{MeHgCl}^w\}}{\phi_w} - \frac{MeHg_{sed} \{f_{MeHg_{DOC}}^{sed} + f_{MeHgCl}^{sed}\}}{\phi_{sed}} \right\} \quad (6) \end{aligned}$$

$$\begin{aligned} \frac{d}{dt} Hg_{tot}^0 = & -k_{ph_{oxy}} L \{Hg_w^0\} + k_{ph_{red}} L_N Hg_w^{II} \{f_{Hg_{DOC}}^w + f_{HgCl_n}^w\} \\ & + k_{ph_{dem}} L_N MeHg_w \{f_{MeHg_{DOC}}^w + f_{MeHgCl}^w\} - k_{vol} \left( Hg_w^0 - \frac{T}{K_{Henry}} Hg_{atm}^0 \right) \quad (7) \end{aligned}$$

$$\begin{aligned} \frac{d}{dt} Hg_{sed}^{II} = & Hg_{sed}^{II} \{v_{s-POM} f_{Hg_{POM}} + v_{s-silt} f_{Hg_{silt}}\} - Hg_{sed}^{II} \{v_{r-POM} f_{Hg_{POM}} + v_{r-silt} f_{Hg_{silt}}\} \\ & + k_{met}^{sed} Q_{10} Hg_{sed}^{II} \{f_{Hg_{DOC}}^{sed} + f_{HgCl_n}^{sed}\} \\ & + k_{demet}^{sed} Q_{10} MeHg_{sed} \{f_{MeHg_{DOC}}^{sed} + f_{MeHgCl}^{sed}\} \\ & + \frac{D_m \phi_{sed}}{z_{sed} / \phi_{sed}} \left\{ \frac{Hg_{sed}^{II} \{f_{Hg_{DOC}}^{sed} + f_{HgCl_n}^{sed}\}}{\phi_w} - \frac{Hg_{sed}^{II} \{f_{Hg_{DOC}}^{sed} + f_{HgCl_n}^{sed}\}}{\phi_{sed}} \right\} \quad (8) \end{aligned}$$

$$\begin{aligned} \frac{d}{dt} MeHg_{sed} = & MeHg_w \{v_{s-POM} f_{MeHg_{POM}}^w + v_{s-silt} f_{MeHg_{silt}}^w\} - MeHg_{sed} \\ & \{v_{r-POM} f_{MeHg_{POM}}^{sed} + v_{r-silt} f_{MeHg_{silt}}^{sed}\} + k_{met}^{sed} Q_{10} Hg_{sed}^{II} \\ & \{f_{Hg_{DOC}}^{sed} + f_{HgCl_n}^{sed}\} - k_{demet}^{sed} Q_{10} MeHg_{sed} \{f_{MeHg_{DOC}}^{sed} + f_{MeHgCl}^{sed}\} \\ & + \frac{D_m \phi_{sed}}{z_{sed} / \phi_{sed}} \left\{ \frac{MeHg_w \{f_{MeHg_{DOC}}^w + f_{MeHgCl}^w\}}{\phi_w} - \frac{MeHg_{sed} \{f_{MeHg_{DOC}}^{sed} + f_{MeHgCl}^{sed}\}}{\phi_{sed}} \right\} \quad (9) \end{aligned}$$

where  $K_D$  is the equilibrium constant for the partitioning process (Table S3),  $\phi$  is the porosity, POM, SILT and DOC indicate the concentrations of POM, silt and DOC, respectively,  $v_s$  is the sinking velocity (Table S5),  $v_r$  is the resuspension velocity (Table S6),  $k_x$  is the kinetic constant a given process (e.g.  $k_{met}$  is for methylation) (Table S4),  $Q_{10}$  is the temperature correction factor for Hg methylation, and  $L_N$  is the adjusted light intensity for photochemical transformations (Table S4). The concentrations of dissolved and particulate Hg species are computed at each model time step from the fractions of Eqs. (1)–(4) and the total concentrations of  $Hg^{II}$ , MeHg and  $Hg^0$  evolving according to Eqs. (5)–(9). The modeled dissolved Hg species includes both complexes of  $Hg^{II}$  and MeHg to DOC ( $Hg_{DOC}$  and  $MeHg_{DOC}$ ) and the ionic phases ( $HgCl_n$  and  $MeHgCl$ ), as well as  $Hg_{(g)}^0$ . The modeled particulate Hg species of  $Hg^{II}$  and MeHg are associated with particulate organic matter ( $Hg_{POM}$  and  $MeHg_{POM}$ ) and silt ( $Hg_{silt}$  and  $MeHg_{silt}$ ). Throughout the manuscript, in order to compare model results and experimental observations, dissolved Hg ( $Hg_D$ ) is used to indicate the sum of all dissolved species ( $Hg^0$ ,  $Hg_{DOC}$ ,  $MeHg_{DOC}$ ,  $HgCl_n$ , and  $MeHgCl$ ), and  $MeHg_D$  to indicate the sum of  $MeHg_{DOC}$  and  $MeHgCl$ . Particulate Hg ( $Hg_P$ ) and MeHg ( $MeHg_P$ ) indicate the sum of  $Hg_{POM}$  and  $Hg_{silt}$  and the sum of  $MeHg_{POM}$  and  $MeHg_{silt}$ , respectively. The sum of all Hg species, including methylated species in dissolved and particulate phases, is hereinafter referred to as the total Hg ( $Hg_T$ ), while the sum of all methylated Hg species ( $MeHg_{DOC}$ ,  $MeHgCl$ ,  $MeHg_{POM}$ ,  $MeHg_{silt}$ ) is referred to as the total MeHg ( $MeHg_T$ ).

## 2.5. Model implementation

The model was implemented by discretizing the Venice Lagoon into 10 sub-basins (Fig. 1) following the partitioning defined through hydrodynamic modeling by Solidoro et al. (2004), which was also used in Sommerfreund et al. (2010). Each sub-basin also included 4 sediment layers that were discretized as in Zonta et al. (2018): layer A (0–5 cm depth), layer B (5–10 cm depth), layer C (10–20 cm depth), and layer D (20–30 cm depth). Initial conditions (Table S7) for Hg and sediment (silt, POM and sand) were set in agreement with the concentrations measured in sediments that were older than 100 years and thus representative of preindustrial levels for the area (see Zonta et al., 2018).

Residual fluxes (Solidoro et al., 2004) were used to force hydrodynamic exchanges among the 10 water boxes in the model and through the marine boundaries. Marine boundary concentrations for  $Hg^{II}$ , MeHg, and  $Hg^0$  (Table S4) were set according to the literature (Bloom et al., 2004; Kotnik et al., 2015). Industrial dumping of Hg to the central-northern lagoon (Section 2.3 and Text S1) was set in the model as a direct input to box 6 that started in 1936. The atmospheric deposition load (Section 2.3) was modeled as homogenous over the lagoon area, while river inputs (Section 2.3) were distributed among model sub-basins 2, 5, 6, 8, and 9 in ways that were proportional to the river runoff (Zuliani et al., 2005). Inputs from the city of Venice were equally divided among sub-basins 3, 5, and 6.

The initial conditions for MeHg<sub>P</sub> in sediment (Table S7) were set by applying the MeHg% observed in the lagoon sediments (Guédrón et al., 2012; Han et al., 2007), which spanned from 0.02% in the southern area to 0.45% in the northern area. The observed MeHg% in sediments (Fig. S5) was also used as a constraint to calibrate MeHg demethylation in sediment, while the Hg methylation rates (Table S7) were set based

on site-specific profiles measured at four stations (Han et al., 2007). The Hg methylation and MeHg demethylation rates in water were calibrated within the ranges of other Mediterranean lagoons and estuaries (Hines et al., 2012; Monperrus et al., 2007a; Sharif et al., 2014), and the Hg methylation rates were assumed to increase with temperature (Table S5). The partition coefficients (Table S3) for Hg and MeHg ( $K_{D-Hg}$  and  $K_{D-MeHg}$ ) were selected from previous investigations in the Venice Lagoon (Guédron et al., 2012; Han et al., 2007). The other model parameters were set in agreement with the literature (Arndt et al., 2013; Hollweg et al., 2010; Soerensen et al., 2016; Solidoro et al., 2005).

Among the environmental factors that likely affected the Hg cycle in the Venice Lagoon, eutrophication occurred during the 1980s (Sfriso and Sfriso, 2017), and sediment resuspension was particularly intense during the 1990s due to the uncontrolled harvesting of *R. philippinarum* (Molinarioli et al., 2013; Sarretta et al., 2010; Sfriso et al., 2005). Clam harvesting was regulated in 2002; however, sediment loss is still a threat to the lagoon ecosystem (Sarretta et al., 2010). Eutrophication was simulated by increasing the primary production rates in the whole lagoon in the period 1980–1990 (Table S6). Homogeneous settling velocities for silt and POM (Table S5) were set for all the model boxes, while the sediment resuspension was assumed to differ spatially among sub-basins (Table S6) that were identified as depositional and erosional by previous studies (Sarretta et al., 2010). In all the sub-basins, the resuspension rate varied during the simulation based on the environmental conditions of the period (Table S6); it was set low at the beginning of the simulation, sharply increased in the 1991–2002 period, and decreased in 2002, when clam harvesting regulations were enacted. Sediment resuspension rates were calibrated to achieve net sediment erosion in the erosional sub-basins during the 1991–2002 period (Fig. S6), while for the more recent period, they were calibrated to match the available observations of SPM and POM concentrations (Figs. S7 and S8) as well as the observed distribution of organic carbon (OC%) (Fig. S9) in surface sediments (Zonta et al., 2018).

### 3. Results and discussion

The results of the estimates of  $Hg_T$  and  $MeHg_T$  emitted from natural and industrial sources (Section 2.3) are provided in Section 3.1, and the

resulting model concentrations are compared with data (Section 3.2) on the  $Hg_T$ ,  $MeHg_T$ ,  $Hg_D$  and  $MeHg_D$  concentrations in water and sediments collected over the years (Section 2.2). The impacts of loadings (Section 2.3), eutrophication and high sediment resuspension (Section 2.5) on the dynamic evolution of  $Hg_T$  and  $MeHg_T$  in the lagoon are discussed in Section 3.3, and the budget for  $Hg_T$  and  $MeHg_T$  in the present state is given in Section 3.4. The impacts of future scenarios of atmospheric deposition (Section 2.3) are presented in Section 3.5.

#### 3.1. Historical Hg emissions and inputs in the Venice area

The cumulative amount of  $Hg_T$  emitted from the industrial site during the 1936–2010 period was estimated to be ~66 Mg, where ~64% (~42 Mg) was emitted to the water and 36% (~23 Mg) was emitted to the atmosphere (Fig. S2). Compared to global estimates (Streets et al., 2017) of cumulative releases (1850–2010) from zinc smelting and soda-chlorine production, the contribution of the Venice area represents ~0.13% of atmospheric emissions and ~0.05% of land/water emissions.

The estimated  $Hg_T$  and  $MeHg_T$  inputs to the Venice Lagoon (Fig. S10) from all natural and anthropogenic sources (i.e., industrial, rivers, atmosphere, and city) since 1900 are ~36 Mg and ~380 kg, respectively. The highest load (~1.5 Mg  $y^{-1}$  of  $Hg_T$  and ~16 kg  $y^{-1}$  of  $MeHg_T$ ) was in 1970, when industrial inputs accounted for more than 80% of the total inputs (Fig. S10). In the present and future states, there is an increasing importance of atmospheric sources (~40% of  $Hg_T$  inputs and ~20% of  $MeHg_T$  inputs), which are more influenced by global dynamics, and riverine sources (~30% of  $Hg_T$  inputs and ~60% of  $MeHg_T$  inputs), which are more influenced by local management, respectively.

#### 3.2. Mercury and methylmercury in lagoon sediment and water

The model outputs simulate the dynamic evolution of the system for 1900–2100, reproducing the concentrations of particulate and dissolved mercury species in water and sediment, which were tested against the data collected in the Venice Lagoon in different periods (Table S1 and Fig. S1), assessing  $Hg_p$  (Figs. 2 and S11) and  $MeHg_p$  (Fig. 3) in sediment,

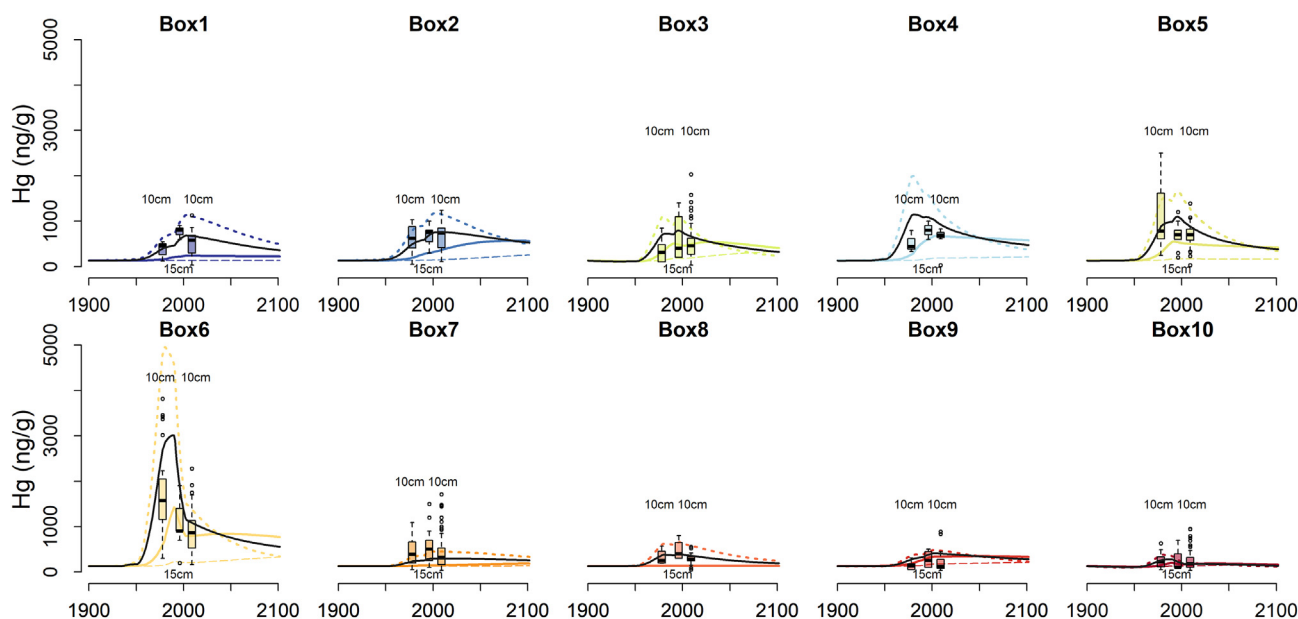


**Fig. 2.** Time evolution (1900–2100) of modeled concentrations of  $Hg_p$  in sediment ( $\mu g g^{-1}$ ) layers A (dotted line, 0–5 cm depth), B (solid line, 5–10 cm depth) and C (dashed line, 10–20 cm depth) in each sub-basin. The black line is the mean of the modeled concentrations for the upper 10 cm (layers A and B). Boxplots show the observed concentrations from sediment cores taken in 1977 in the upper 10 cm (Donazzolo et al., 1984), sediment cores taken in 1997 in the upper 15 cm (MAV-CVN, 1999), and sediment cores taken in 2008 at the 0–5 cm and 5–10 cm depths (Zonta et al., 2018). Boxplots indicate the median, the 1st and 4th quartiles and the extremes of the observations. The horizontal dashed gray line indicates the sediment legislative limit of  $0.3 \mu g g^{-1}$ .

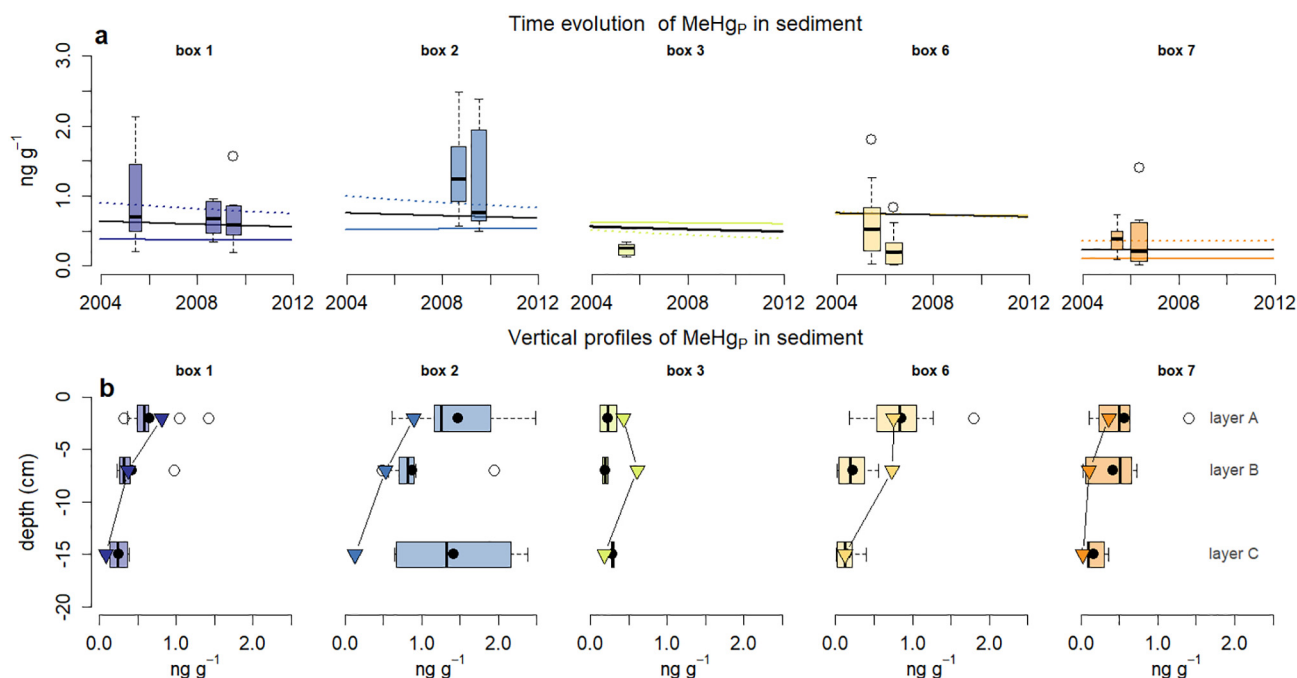


**Fig. 3.** Modeled concentrations of MeHg<sub>P</sub> in sediment (ng g<sup>-1</sup>) of boxes 1, 2, 3, 6, and 7 compared with the observations (boxplots) from sediment cores taken in 2005 (Han et al., 2007) and 2006 (Kim et al., 2011) in the top 20 cm depth and in 2008–2009 (Guédron et al., 2012) in the 10 cm depth. Boxplots indicate the median, the 1st and 4th quartiles and the extremes of the observations; a) upper panels show the comparison with the modeled time evolution (1900–2100) in layers A (dotted line, 0–5 cm depth) and B (solid line, 5–10 cm depth). The black line is the mean of the modeled concentrations at the 10 cm depth (layers A and B); b) lower panels show the comparison with the modeled vertical profiles (reverse triangles).

Hg<sub>D</sub> and MeHg<sub>D</sub> in porewater (Fig. S12) and Hg<sub>T</sub>, MeHg<sub>T</sub>, Hg<sub>D</sub> and MeHg<sub>D</sub> in water (Fig. 4).

The time evolutions of the modeled Hg<sub>P</sub> concentrations in sediment layers A–C of each sub-basin are shown in Fig. 2, and the values were compared with the observations from three basin-scale assessments carried out in 1977 (Donazzolo et al., 1984), 2005 (MAV, 1995) and 2008 (Zonta et al., 2018). Despite the very good temporal and spatial resolution of these datasets, the comparison is not straightforward because these studies analyzed sediment cores of different thicknesses (0–10 cm depth, 0–15 cm depth, and 0–40 cm depth sliced at 5- and 10-cm intervals); however, it can be seen from Fig. 2 that the modeled sediment Hg<sub>P</sub> concentrations overall adequately reproduced the time evolution and spatial distribution of the observed concentrations. Furthermore, a comparison was made between the simulated Hg<sub>P</sub> concentration vertical profiles in the sediments (Fig. S11) and the 2008 observations (Zonta et al., 2018) for layers A (0–5 cm depth), B (5–10 cm depth), C (10–20 cm depth) and D (20–30 cm depth). The model agrees with the observed spatial distribution of Hg<sub>P</sub> concentrations in the sediments, with a high correlation in layers A (Pearson's correlation,  $r = 0.96$ ,  $p < 0.01$ ) and B ( $r = 0.75$ ,  $p < 0.01$ ), and a weaker correlation with the deep sediment observations (layer C,  $r = 0.50$ , n.s.; and layer D,  $r = 0.23$ , n.s.). The simulated sediment Hg<sub>P</sub> concentrations tended to slightly overestimate the median concentrations observed in surface layer A (root-mean-square error, RMSE =  $0.77 \mu\text{g g}^{-1}$ ) and underestimate the median concentrations in layers B (RMSE =  $0.51 \mu\text{g g}^{-1}$ ), C and D (RMSE =  $0.41 \mu\text{g g}^{-1}$  and  $0.33 \mu\text{g g}^{-1}$ ), suggesting that sediment burial and/or remixing is somewhat underestimated, especially in the northern area. This result can be attributed to the absence of natural and anthropogenic processes in the model that cause sediment reworking, such as bioturbation and sediment dredging, which have a strong impact on the profiles of pollutants (Zonta et al., 2018). An underestimation in our reconstruction of past Hg inputs to the lagoon may also explain the model-observation mismatch in the deep sediment layers. Considering each box vertical profile (Fig. S11), the RMSE was highest in box 6

(RMSE =  $0.57 \mu\text{g g}^{-1}$ ), which is the most enriched in Hg, and lowest in box 10 (RMSE =  $0.11 \mu\text{g g}^{-1}$ ), which is located the farthest from Hg sources.

The modeled vertical profiles of the Hg<sub>D</sub> and MeHg<sub>D</sub> concentrations in pore water (Fig. S12) tended to be lower than those of the observations (Guédron et al., 2012; Han et al., 2007). The underestimation is likely due to the lack of diagenetic processes in the sediment model, the importance of which is highlighted by the field data of pore water that display subsurface maxima, either in layer B or layer C, at most of the stations.

The modeled MeHg<sub>P</sub> concentrations in sediment layers A–C are shown in Fig. 3, and they are compared with the limited number of available observations (Table S1) for the northern (Guédron et al., 2012; Han et al., 2007) and central lagoon (Han et al., 2007; Kim et al., 2011). The modeled sediment MeHg<sub>P</sub> concentrations (Fig. 3a) were in the range of observations for 2005 (Han et al., 2007), 2006 (Kim et al., 2011), 2008 and 2009 (Guédron et al., 2012); the exception was sub-basin 3, where the model slightly overestimated the observations. The modeled vertical profiles of the MeHg<sub>P</sub> concentrations (Fig. 3b) for 2005–2009 in sediment layers A–C were in satisfactory agreement ( $r = 0.79$ , n.s., RMSE =  $0.57 \text{ ng g}^{-1}$ ) with the average observation values for the corresponding years and sediment layers (Guédron et al., 2012; Han et al., 2007; Kim et al., 2011). The modeled MeHg<sub>P</sub> concentrations in the surface sediment were highly correlated with the Hg<sub>P</sub> concentrations ( $r = 0.9$ ,  $p < 0.01$ ), which was in agreement with the findings of Han et al. (2007) for the Venice Lagoon ( $r = 0.96$ ,  $p < 0.05$ ).

The modeled water concentrations of Hg<sub>T</sub>, Hg<sub>D</sub>, MeHg<sub>T</sub>, and MeHg<sub>D</sub> were compared to the observations (Fig. 4) from 2001 to 2003 in the northern, central and southern parts of the lagoon (Bloom et al., 2004) and compared to the Hg<sub>D</sub> and MeHg<sub>D</sub> concentrations measured in 2009–2010 in the central lagoon (MAV-CORILA, 2011). The modeled water concentrations showed recoveries of Hg<sub>T</sub>, Hg<sub>D</sub>, and, to a lesser extent, MeHg<sub>T</sub> and MeHg<sub>D</sub> at the end of 2002, when sediment resuspension decreased due to clam harvesting regulations.

The modeled Hg<sub>T</sub> and MeHg<sub>T</sub> concentrations in water (Fig. 4) were comparable with the 2002 observations (Bloom et al., 2004).

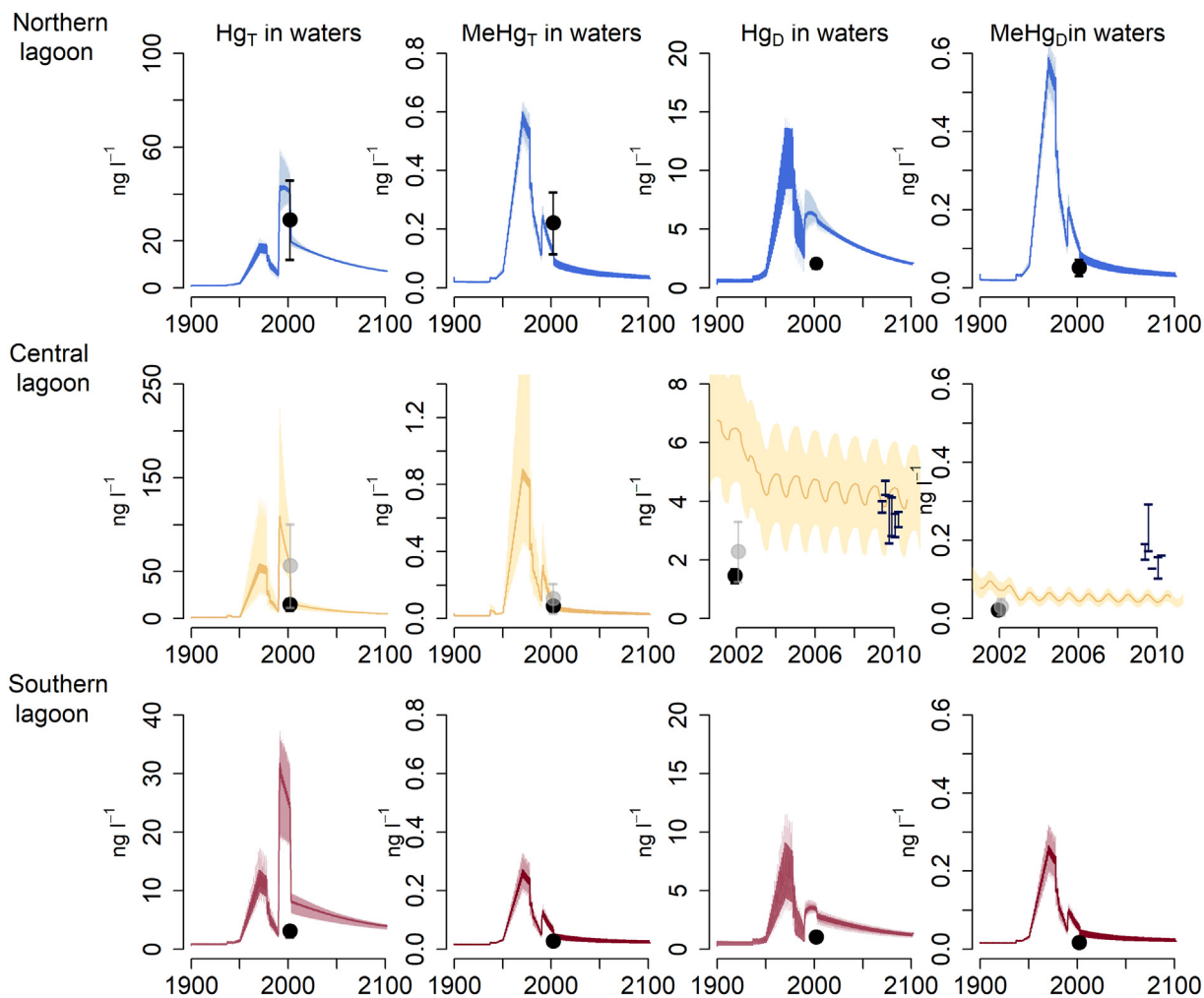


**Fig. 4.** Modeled (colored lines = mean and areas = variability) and observed (dots and segments)  $Hg_T$ ,  $MeHg_T$ ,  $Hg_D$  and  $MeHg_D$  concentrations in the water of the northern (upper panels), central (central panels) and southern (lower panels) parts of the lagoon. Gray dots and bars indicate the concentrations measured in the lagoon water close to the Marghera industrial site. Black dots represent data sampled in 2001–2003 (Bloom et al., 2004), and dark blue segments represent data sampled in 2009 (MAV-CORILA, 2011). The northern lagoon includes boxes 1, 2 and 4, the central lagoon includes boxes 3, 5, 6, and 7, and the southern lagoon includes boxes 8, 9 and 10. Note that the plots of  $Hg_D$  and  $MeHg_D$  in the central lagoon have a different timescale. (For interpretation of the references to colour in this figure legend, the reader is referred to the web version of this article.)

The modeled  $Hg_D$  concentrations (Fig. 4) tended to overestimate the 2002 observations (Bloom et al., 2004) and were in good agreement with the 2009–2010 observations in the central lagoon (MAV-CORILA, 2011); however, the modeled  $MeHg_D$  concentrations tended to overestimate the 2002 observations (Bloom et al., 2004) and underestimate the 2009–2010 observations (MAV-CORILA, 2011). Higher error in the dissolved phase might be due to the fact that the values for partition coefficients ( $K_D$ , Table S3) are maintained constant throughout the simulation and used for both water and sediment boxes. Experimental studies show that  $K_D$  values differ among compartments and can vary during the year (Schartup et al., 2015a, 2015b; Hines et al., 2012). This model feature limits the capability to describe the different physicochemical conditions of water and sediment affecting mercury partitioning, but it also prevents the over-tuning of model parameters, and a tradeoff must be found to obtain acceptable agreement for both water and sediment dynamics. The modeled  $MeHg_T$  and  $MeHg_D$  concentrations in the lagoon water followed a seasonal cycle with summer maxima (31–60% higher than that in winter) driven by the higher methylation activity; the modeled  $Hg_T$  and  $Hg_D$  concentrations also slightly increased during summer (1–3%) due to the highest  $MeHg$  and  $Hg^0$  concentrations. The modeled summer increase in  $MeHg$  concentrations agreed with the observation by Bloom et al. (2004), who, in contrast with our results, found a strong increase in  $Hg_T$  during summer in relation

to a higher SPM. The model presented here simulated an average re-suspension throughout the year, which did not account for seasonal variations and extreme events. To reproduce the actual pattern of sediment dynamics, a fully coupled hydrodynamic-sediment-biogeochemical model with a finer spatial resolution would be needed. Indeed, in shallow basins such as the Venice Lagoon, benthic-pelagic coupling is of great importance and is highly variable during the year. However, the implementation of a model at a higher spatial resolution, such as finite difference or finite element models, which have already been applied to the Lagoon of Venice in hydrodynamic and biogeochemical studies (Solidoro et al., 2005; Umgiesser et al., 2004, 2003), would require too much computation time to explore the long-term dynamics at the investigated time scale.

### 3.3. Hg cycling in the changing environment of the Venice Lagoon

In the Venice Lagoon, the time evolutions of the  $Hg_T$  and  $MeHg_T$  reservoirs, fluxes (Fig. 5) and concentrations (Fig. 6) result from the combined effects of both variations in Hg emissions and inputs over time (Section 2.3) and strong changes in environmental conditions triggered by human activities. According to the modeled dynamics, on the one hand, eutrophication (Sfriso and Sfriso, 2017; Solidoro et al., 2010) drove an increase in  $Hg_P$  deposition flux toward the seafloor; on the other hand, during the following period of high sediment resuspension

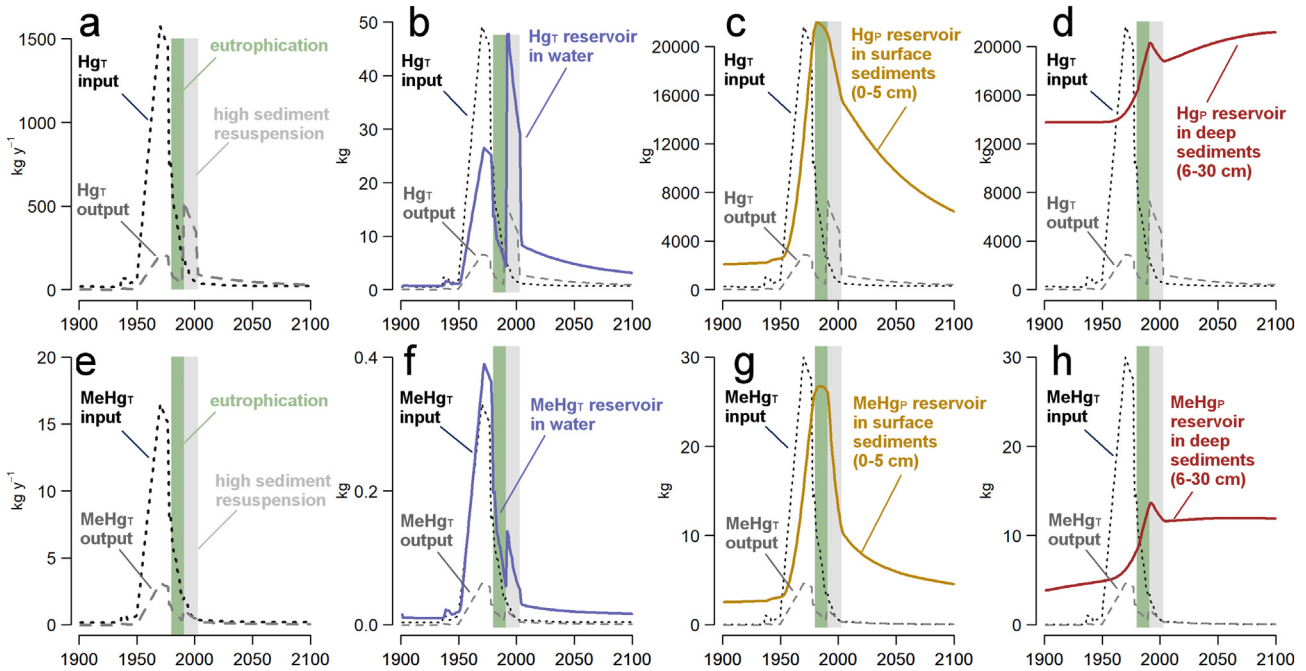


**Fig. 5.** Time evolution of modeled dynamics from the preindustrial (1900–1935) to the postindustrial phases (2005–2100):  $Hg_T$  inputs from industrial, riverine, atmospheric, and urban sources to the Venice Lagoon and outputs due to tidal outflow and volatilization ( $kg\ y^{-1}$ ); b)  $Hg_T$  water reservoirs (kg); c)  $Hg_T$  sediment reservoirs (kg); d)  $MeHg_T$  inputs to the Venice Lagoon from industrial riverine, atmospheric, and urban sources and outputs due to tidal outflow at the inlets ( $kg\ y^{-1}$ ); e)  $MeHg_T$  water reservoirs (kg); and f)  $MeHg_T$  sediment reservoirs (kg). Green rectangles indicate the eutrophication period (1980–1990), and gray rectangles indicate the period of increased resuspension (1990–2002). (For interpretation of the references to colour in this figure legend, the reader is referred to the web version of this article.)

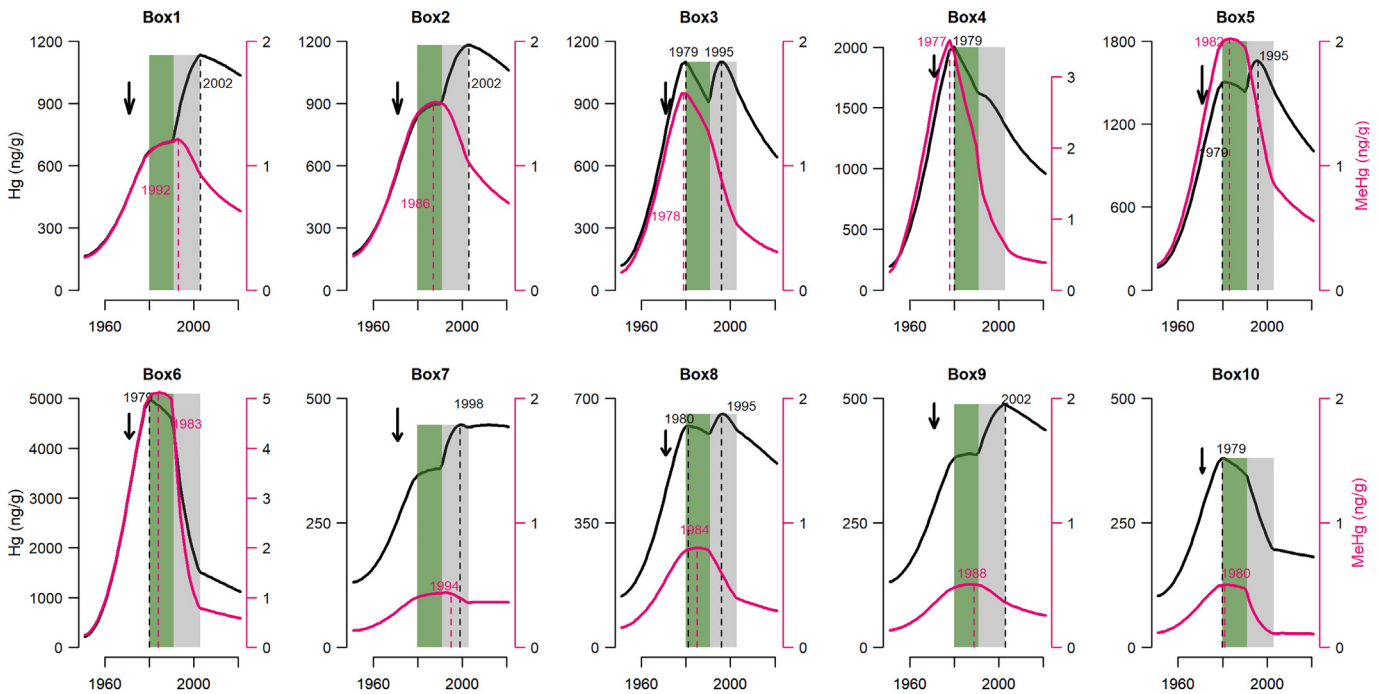


**Fig. 6.** Time evolution in each sub-basin of modeled concentrations of  $Hg_P$  (black lines) and  $MeHg_P$  (pink lines) in sediment layer A (0–5 cm), zoomed for the period 1950–2020. The black arrows indicate the year of maximum  $Hg$  inputs. Green rectangles indicate the eutrophication period (1980–1990), and gray rectangles indicate the period of increased resuspension (1980–2002). Right axes are for  $MeHg$ , and left axes are for  $Hg$ . It should be noted that each plot has a different scale. (For interpretation of the references to colour in this figure legend, the reader is referred to the web version of this article.)

due to the unregulated harvesting of Manila clams (Sfriso et al., 2005; Solidoro et al., 2000), the sediment of the lagoon became a secondary  $Hg_P$  source for the lagoon water through the remobilization of previously accumulated  $Hg_P$ .

The maximum of the modeled surface sediment  $Hg_P$  reservoir ( $\sim 22\ Mg$ ) was reached in 1982 (Fig. 5c), approximately ten years after the maximum  $Hg_T$  inputs (1970) occurred; this result is because the eutrophication during the 1980s triggered an enhancement in POM

deposition (Fig. S9), consequently increasing the vertical transport of  $Hg_{POM}$  from the water to the seafloor. Later, in the 1980s, as eutrophication continued to affect the system, sediment deposition was still high, and the Hg inputs from the watershed and atmosphere continued to decrease (Fig. 5a), leading to a slight decrease in the surface sediment  $Hg_P$  reservoir ( $\sim 21$  Mg, Fig. 5c) and an increase in the  $Hg_P$  reservoir in the deepest sediment depths ( $\sim 20$  Mg in sediment layers B–D, Fig. 5d) due to the burial of the most polluted sediments below the new sediments with lower  $Hg_P$  concentrations. In 1991, the  $Hg_P$  accumulated in sediment at all depths and reached its maximum value of  $\sim 41$  Mg. This increase in burial has also been observed in the Baltic Sea under eutrophic conditions (Soerensen et al., 2016).

At the beginning of the 1990s, despite the continued declining trend of  $Hg_T$  inputs from the watershed, the modeled  $Hg_T$  water reservoir (Fig. 5b) sharply increased (up to  $\sim 48$  kg), and the  $Hg_P$  surface sediment reservoir decreased (Fig. 5c) due to the abrupt increase in sediment resuspension (Table S6) that remobilized the  $Hg_P$  from the sediments to the water column. The increased water  $Hg_T$  concentrations (Fig. 5b) drove an increase in the export of  $Hg_T$  from the lagoon (Fig. 5a) through transport at the lagoon inlets and evasion of  $Hg^0$ ; however, it also caused a redistribution of Hg from the most contaminated central area to the less contaminated northern and southern areas (Figs. 2 and 6), as has been observed by other authors (Bernardello et al., 2006; Masiol et al., 2014; Molinaroli et al., 2013; Zonta et al., 2018).

The spatial variability in the  $Hg_P$  sediment concentrations among sub-basins (Fig. 6) depends on the balance among different processes: Hg loadings, net sediment deposition or resuspension, and sediment transport. At the end of the 1970s, the surface sediment  $Hg_P$  concentrations in central sub-basin 6, which received the industrial load, were

$\sim 10$  times higher than the concentrations in the southern sub-basins. The southern sub-basins (8–10) presented the lowest sediment  $Hg_P$  concentrations due to the combination of negligible industrial, urban and river inputs and the richer sediment texture in sand, which has a lower affinity for Hg species (Acquavita et al., 2012; Guédron et al., 2012; Lamborg et al., 2016; Zonta et al., 2018). The northern sub-basins 1, 2 and 4 were influenced the most by river Hg loading, as 46% of river runoff flows into sub-basin 2. The Hg loading to the other central-northern sub-basins (3 and 5) came from urban discharge and hydrological exchange with neighboring sub-basins. During the 1990s, the recovery from eutrophication and intensification of sediment resuspension caused severe erosion in sub-basins 6 and 10 and moderate erosion in sub-basins 3, 5, 7 and 8 (Fig. S6). In sub-basins 6 and 10, the  $Hg_P$  surface sediment concentrations sharply decreased (Fig. 6), and  $Hg_P$  was transported elsewhere:  $Hg_P$  concentrations sharply increased in the northern sub-basins (1 and 2) and moderately increased in the southern sub-basins (7, 8, 9). Sub-basins 3 and 5 were initially affected by highly polluted sediment transported from sub-basin 6, and the  $Hg_P$  concentrations of these sub-basins increased to the maximum value in 1995, followed by a decrease due to continued erosion (Fig. 6).

The modeled time evolution of  $MeHg_T$  reservoirs (Fig. 5e–h) was similar to that of  $Hg_P$ , although it was less influenced by sediment resuspension and transport. The peak in the water reservoir during the 1990s (0.14 kg) was less pronounced (Fig. 5f) because of a weaker affinity of  $MeHg$  to sediments (lower  $K_D$ , Tables S3) and possibly because of demethylation that occurred in the water column. In contrast to  $Hg_T$ , the modeled water  $MeHg_T$  reservoir was maximum (0.39 kg) when inputs were highest (Fig. 5f) during the 1970s, and the modeled sediment  $MeHg_P$  concentrations (Fig. 6) peaked during the eutrophication

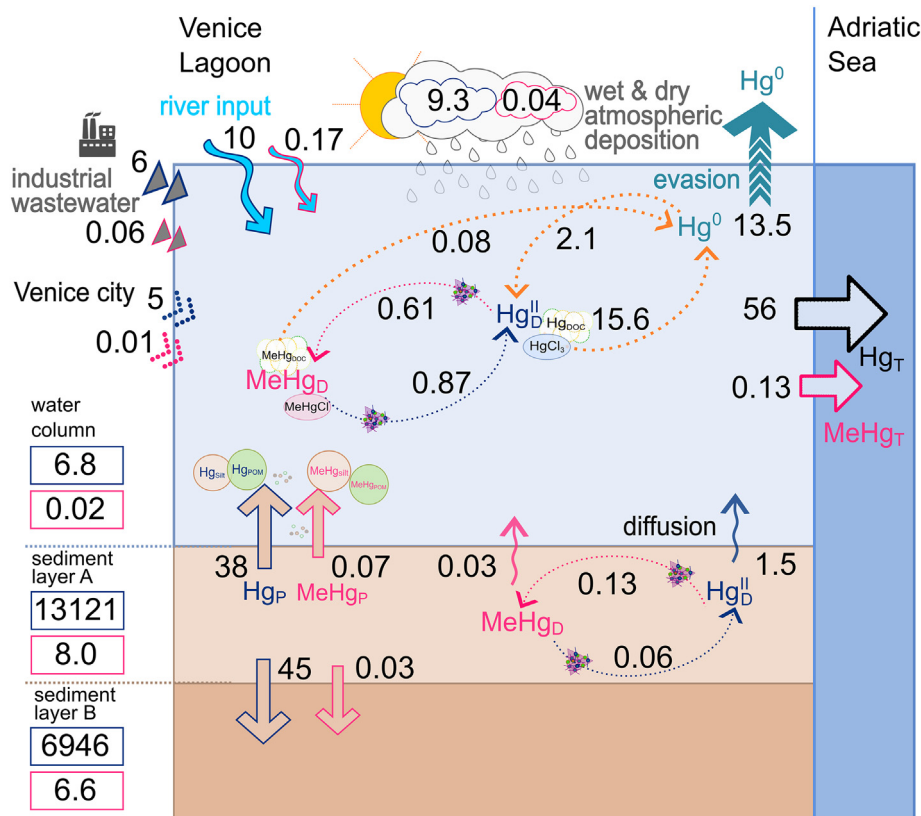


**Fig. 7.** Budget for Hg species in the Venice Lagoon in its present state (2019). Fluxes of Hg species ( $kg\ y^{-1}$ ) among compartments are indicated by arrows and numbers, as described in Fig. S4. Modeled reservoirs (kg) of  $Hg^{II}$  (blue) and  $MeHg_T$  (pink) species in the water and sediment layers are given in the rectangles on the left side.  $Hg^0$  (dark cyan) is produced upon net photoreduction in the water column and mostly evades to the atmosphere. Net sediment resuspension and burial of  $Hg_P$  and  $MeHg_P$  are indicated by the brown arrows. The fluffy arrows represent diffusion of  $Hg_D$  and  $MeHg_D$  from sediment. Dashed arrows indicate microbial Hg methylation,  $MeHg$  demethylation and photochemical transformations (photoreduction, photooxidation, photodemethylation). Thick arrows show exports to the Adriatic Sea and to the atmosphere. (For interpretation of the references to colour in this figure legend, the reader is referred to the web version of this article.)

phase (1980–1989) in all the sub-basins and did not exhibit secondary peaks in the late 1990s.

### 3.4. Postindustrial phase and current budget for $Hg_T$ and $MeHg_T$

In the current postindustrial phase, the estimated budget for Hg species in the Venice Lagoon for 2019 (Fig. 7) showed that the estimated  $Hg_T$  outputs (approximately  $70 \text{ kg y}^{-1}$ ) slightly exceeded the estimated inputs to the water column from the watershed and sediments, causing a slow decrease in  $Hg_T$  concentrations over time (Fig. 2). The main flux to the lagoon water was from the sediment acting as a secondary source through the net resuspension of  $Hg_p$  ( $\sim 38 \text{ kg y}^{-1}$ ), while the  $Hg_D$  diffusion from pore water was much smaller ( $\sim 1.5 \text{ kg y}^{-1}$ ). The largest inputs from the watershed were rivers ( $\sim 10 \text{ kg y}^{-1}$ ) and atmospheric deposition ( $\sim 9.3 \text{ kg y}^{-1}$ ); in addition,  $\sim 6 \text{ kg y}^{-1}$  was dumped from the industrial area, and  $\sim 5 \text{ kg y}^{-1}$  was exported from the Venice city channels to the lagoon. Approximately  $56 \text{ kg y}^{-1}$  of  $Hg_T$  is exported to the Adriatic Sea (Mediterranean Sea) through tidal outflow. A further  $\sim 13.5 \text{ kg y}^{-1}$  of  $Hg^0$  is lost from the system through evasion. The modeled export to the Adriatic Sea accounted for  $\sim 4.3\%$  of the inputs to the Mediterranean Sea from point sources ( $1.3 \text{ Mg y}^{-1}$ ) estimated for 2020 (Rajar et al., 2007) and for 0.01–0.04% of the estimated Hg releases from coastal areas to the open ocean, which is  $50\text{--}10 \text{ Mg y}^{-1}$  globally (Kocman et al., 2013). However, considering that this budget was calculated based on residual fluxes computed under climatological conditions, i.e., it did not consider extreme events, this value is likely a lower bound. The  $Hg_T$  export estimated based on the 2001–2003 assessment (Bloom et al., 2004) that set the water outflow to  $1.4 \cdot 10^{11} \text{ m}^3 \text{ y}^{-1}$  in agreement with the estimate from Critto and Marcomini (2001) is much higher ( $\sim 1110 \text{ kg y}^{-1}$ ) than the estimate used in this work made with the validated Shyfer model (Solidoro et al., 2004), which computed a net outflow value of  $\sim 1.5 \cdot 10^9 \text{ m}^3 \text{ y}^{-1}$ . The  $Hg_T$  exported to the Adriatic Sea modeled for 2019 is  $\sim 3$  times lower than the export modeled for 1970 (maximum inputs) and  $\sim 7$  times lower than the export modeled during the 1990s (due to high sediment resuspension). According to the modeled dynamics, sediment will continue to act as a secondary source in the long run, with the continuous mobilization of  $Hg_p$  to the lagoon water leading to decreasing concentrations and fluxes in the whole system, as Hg is transferred to the water column and transported to the Adriatic Sea through water outflow.

In the modeled 2019 budget (Fig. 7), the inputs of  $MeHg_T$  to the water column ( $\sim 1.0 \text{ kg y}^{-1}$ ) were almost balanced with the outputs ( $\sim 1.1 \text{ kg y}^{-1}$ ), and the  $MeHg$  concentrations slowly decreased over time. Biological demethylation exceeded biological  $Hg_D$  methylation by  $\sim 0.26 \text{ kg y}^{-1}$  in the water, where  $\sim 0.08 \text{ kg y}^{-1}$  of  $MeHg_D$  was further degraded by photodemethylation; however, net  $Hg_D$  methylation prevailed in the sediment ( $\sim 0.07 \text{ kg y}^{-1}$ ). The main source of  $MeHg_T$  in the lagoon water is inputs from the watershed ( $\sim 0.28 \text{ kg y}^{-1}$ ), but net sediment resuspension is also relevant ( $\sim 0.07 \text{ kg y}^{-1}$  of  $MeHg_p$ ), while  $MeHg_D$  inputs from pore water diffusion ( $\sim 3 \cdot 10^{-2} \text{ kg y}^{-1}$ ) are small. Fluxes from pore water may be higher due to the occurrence of processes that are not included in this model, as well as in most Hg models that are state of the art: according to Guédron et al. (2012), in the shallower lagoon areas, the wave shear stress acting on the surface sediment during tidal flooding causes advective flows and oscillations in redox conditions, which lead to the release of dissolved Hg species and to the increase in water concentrations.

Further studies are needed to address the relative importance of in situ versus land-based  $MeHg$  sources, which have been shown to have different bioavailabilities (Bravo et al., 2017; Schartup et al., 2015b). This study suggests that the watershed is an important source of  $MeHg_T$ , implying that a significant portion of  $MeHg$  in the lagoon may not be bioavailable for bioaccumulation. Nonetheless, the Hg and  $MeHg$  concentrations in seston (20–200  $\mu\text{m}$ ) in the Venice Lagoon (Dominik et al., 2014) are much higher than concentrations measured in seston of comparable size in unpolluted areas such as the Gulf of

Lion (Cossa et al., 2012) or the Gulf of Maine (Harding et al., 2018). The relatively low in situ Hg methylation in the Venice Lagoon appears to result in low sediment  $MeHg_p$  concentrations ( $0.01\text{--}2.5 \text{ ng g}^{-1}$ ), which are comparable to concentrations observed at sites with lower  $Hg_T$  levels, such as the Thau Lagoon and Chesapeake Bay (Hollweg et al., 2009; Muresan et al., 2007). However, it should be borne in mind that only a limited number of data describing  $MeHg$  in the Venice Lagoon is available, and it is possible that higher  $MeHg$  concentrations occur in some overlooked areas. For instance, salt marshes have high methylation potential, but limited observations are available for these ecosystems (Gilmour et al., 2018).

### 3.5. Future trends and scenario analysis

Under the Reference scenario (Section 2.3), the modeled concentrations of Hg species decreased over the long term in all sub-basins. By 2100, the decrease in  $Hg_T$  concentrations relative to 2019 was, on average, 53% in water (ranging from 37%–65%) and 53% in surface sediment (layer A) (ranging from 24%–70%). The decrease in  $MeHg_T$  concentrations was slower, 39% (26%–49%) in water and 46% (18%–62%) in surface sediment.

The target concentrations for sediment quality ( $<0.3 \mu\text{g g}^{-1}$  of  $Hg_p$ ) were reached before 2100 only in the southern boxes (boxes 8–10) and box 3 (Table S9). In the northern boxes (1, 2 and 4), the  $Hg_p$  concentrations at the end of the simulation (2100) ranged from  $0.39\text{--}0.49 \mu\text{g g}^{-1}$ , and it took 23–45 years longer to reach the target concentration of  $0.3 \mu\text{g g}^{-1}$ , assuming a constant recovery rate after the end of the simulation. In boxes 5–7, the  $Hg_p$  concentrations at the end of the century spanned from  $0.33$  to  $0.35 \mu\text{g g}^{-1}$ , and the sediment target concentrations were reached between 2113 and 2125 (Table S9). The estimated recovery times, calculated as the time to reach the target concentrations from 2019, averaged 80 years considering all lagoon boxes (Table S9); they were comparable to the recovery times estimated for the Penobscot estuary (Santschi et al., 2017) and lower than those estimated for the Marano–Grado Lagoon (Canu and Rosati, 2017), which has higher Hg concentrations in sediment.

The impacts of scenarios of future atmospheric deposition (Section 2.3 and Fig. 8) on the evolution of the  $Hg_p$  and  $MeHg_p$  concentrations and on the estimated sediment  $Hg_p$  recovery times are shown in Fig. S8 and Table S9, respectively. While an overall decreasing trend was maintained in all scenarios, the two scenarios with increasing atmospheric deposition (“Constant Emissions - B1” +0.42% per year, and “Business-as-Usual - A1B1” +1.79% per year) resulted in slower recovery from Hg pollution and thus higher  $Hg_T$  and  $MeHg_T$  concentrations in 2100 than in the Reference scenario, while the two scenarios with decreasing atmospheric deposition (“Emissions Control - EC” –0.42% per year, and “Zero Emissions - ZE” –0.84% per year) resulted in faster recovery rates. The average recovery time of 80 years estimated for the sediment of the lagoon boxes varied under the two extreme scenarios, with an increase to 87 years for the A1B1 scenario and a decrease to 77 years under the ZE scenario (Table S9). Under the EC scenario, the water concentrations of  $Hg_T$  and  $MeHg_T$  at the end of the century were, on average, 2.1% and 2.3% lower, respectively, than the concentrations in the Reference simulation (Fig. S8), and the sediment concentrations were reduced by 1.4% and 1.6%, respectively. In the ZE scenario, the modeled water concentrations were 5.3% lower in  $Hg_T$  and 5.2% lower in  $MeHg_T$ , while the sediment concentrations were reduced by 3.9% for  $Hg_p$  and by 4.0% for  $MeHg_p$ . In the B1 scenario, the modeled  $Hg_T$  and  $MeHg_T$  water concentrations increased, on average, by 2.1% and 2.3%, respectively, and the sediment concentrations were 1.3% and 1.5% higher for  $Hg_p$  and  $MeHg_p$ , respectively; under the A1B1 scenario, the modeled water concentrations increased by 8.2% for  $Hg_T$  and by 9.4% for  $MeHg_T$ , while the sediment concentrations were 5.2% higher in  $Hg_p$  and 6.1% higher in  $MeHg_p$ .

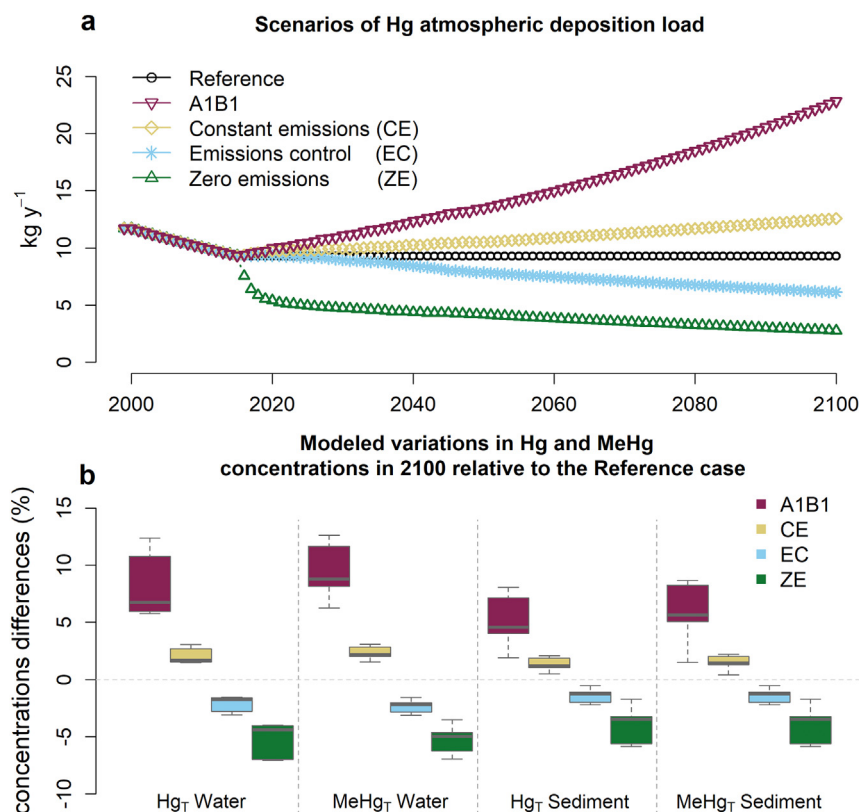


**Fig. 8.** a) Scenarios of atmospheric deposition for 2015–2100 implemented according to Chen et al. (2018), b) variations induced by the scenarios in the modeled Hg and MeHg concentrations in water and sediment in 2100.

#### 4. Conclusions

The integration of field data from various sources sampled in the last 40 years (Section 2.2) into a dynamic biogeochemical model (Section 2.4) enabled us to explore the evolution of the Hg cycle in the Venice Lagoon from the preindustrial period to the end of the century (1900–2100). Changing emissions and  $Hg_T$  and  $MeHg_T$  inputs to the lagoon were estimated (Section 2.3) for the period investigated, providing the first long-term estimate for the area (Section 3.1), and the impacts of these loads and well-documented past alterations of the lagoon ecosystem (Section 2.5) on the Hg dynamics were explored (Section 3.3). The model was used to test hypothesis that the role of the Venice Lagoon sediment as a sink or source for anthropogenic Hg has changed over time as a result of several concurring processes, in particular: the lagoon trophic conditions, the lagoon uses and to the global atmospheric deposition. Confirming the hypothesis, the model suggests that the assessment of  $Hg_T$  and  $MeHg_T$  dynamics, and of the resulting ecosystem exposure, cannot rely only on scattered observations but should be supported by an overall analysis of the other interacting processes. Though limited by inherent modeling simplifications and assumptions, the results of this work showed that the reconstruction of past dynamics based on an ecosystem approach could serve as a basis for understanding of the present distribution of pollutants, highlighting the importance of using sediment dynamics to characterize the role of sediments as pollutant sinks or sources.

In the Venice Lagoon, inputs were highest in the 1970s, when industrial inputs to the lagoon accounted for more than 80% of the total  $Hg_T$  inputs, while in the current postindustrial phase (2019) (Section 3.4), the sediments act as a secondary source, being the main source of  $Hg_T$  for the lagoon waters. The most relevant external  $Hg_T$  sources are rivers and atmospheric deposition, while  $MeHg_T$  seems to be delivered mostly from the watershed, although it is also produced in sediments and resuspended. According to the modeled budgets, the lagoon received

approximately 36 Mg of  $Hg_T$ , including ~380 kg of  $MeHg_T$  in the last century, which has been partially stored in the sediments and is now slowly being released to the lagoon waters and to the Adriatic Sea (~56 kg  $y^{-1}$ , including ~0.13 kg  $y^{-1}$  of  $MeHg$ ), leading to a slow decrease in Hg concentrations.

The modeled spatial and temporal distributions of Hg species (Section 3.2) in lagoon sediment and water are consistent with the available observations from different periods. However, while the evolution of the  $Hg_P$  concentrations in lagoon sediments has been tracked since the 1970s by various studies carried out at the basin scale, there is limited experimental knowledge on the spatial and temporal distribution of  $MeHg$  in the lagoon. The analysis of Hg and  $MeHg$  reservoirs and fluxes reveals the importance of changes in environmental conditions that have driven variations in Hg fluxes (Section 3.3). On the one hand, eutrophication has enhanced sediment deposition to the seafloor, causing the highest accumulation of Hg in sediment when Hg inputs were already declining; on the other hand, uncontrolled Manila clam harvesting during the 1990s enhanced sediment resuspension, leading to mobilization of Hg from the sediments that became a secondary source to the lagoon water and consequently to the Adriatic Sea (Mediterranean Sea), also leading to the redistribution of Hg from the central lagoon to the northern and southern areas.

Although the Hg dynamics in the Venice Lagoon are currently driven by  $Hg_P$  accumulation and remobilization from sediment, the scenario analysis shows that future levels of atmospheric deposition will affect the ambient concentrations of  $Hg_T$  and  $MeHg_T$  and the recovery time for  $Hg_P$  in sediments, suggesting that global policies on Hg emissions reduction are relevant even in polluted ecosystems.

#### Credit authorship contribution statement

b Conceptualization, Data curation, Formal analysis, Investigation, Methodology, Software, Visualization, Writing - original draft, Writing

- review & editing. **Cosimo Solidoro**: Conceptualization, Investigation, Methodology, Supervision, Visualization, Writing - original draft, Writing - review & editing. **Donata Canu**: Conceptualization, Data curation, Formal analysis, Funding acquisition, Investigation, Methodology, Project administration, Resources, Software, Supervision, Writing - original draft, Writing - review & editing.

### Declaration of competing interest

The authors declare that they have no known competing financial interests or personal relationships that could have appeared to influence the work reported in this paper.

### Acknowledgment

This research activity was performed with the contribution of the Provveditorato for the Public Works of Veneto, Trentino Alto Adige and Friuli Venezia Giulia, provided through the concessionary of State Consorzio Venezia Nuova and coordinated by CORILA, and by the Flagship RITMARE - La Ricerca Italiana per il MARE The Italian Research for the Sea, coordinated by the National Research Council and funded by the Ministry of Education, University and Research. The authors declare no conflict of interest.

### Appendix A. Supplementary data

Supplementary data to this article can be found online at <https://doi.org/10.1016/j.scitotenv.2020.140586>.

### References

- Acquavita, A., Covelli, S., Emili, A., Berto, D., Faganelli, J., Giani, M., Horvat, M., Koron, N., Rampazzo, F., 2012. Mercury in the sediments of the Marano and Grado Lagoon (northern Adriatic Sea): sources, distribution and speciation. *Estuar. Coast. Shelf Sci.* 113, 20–31. <https://doi.org/10.1016/j.ecss.2012.02.012>.
- Alava, J.J., Cheung, W.W.L., Ross, P.S., Sumaila, U.R., 2017. Climate change-contaminant interactions in marine food webs: toward a conceptual framework. *Glob. Chang. Biol.* 23, 3984–4001. <https://doi.org/10.1111/gcb.13667>.
- AMAP/UNEP, 2013. *Technical Background Report for the Global Mercury Assessment 2013*. Oslo, Norway / UNEP Chemicals Branch, Geneva, Switzerland.
- Amos, H.M., Jacob, D.J., Streets, D.G., Sunderland, E.M., 2013. Legacy impacts of all-time anthropogenic emissions on the global mercury cycle. *Glob. Biogeochem. Cycles* 27, 410–421. <https://doi.org/10.1002/gbc.20040>.
- Amos, H.M., Jacob, D.J., Kocman, D., Horowitz, H.M., Zhang, Y., Dutkiewicz, S., Horvat, M., Corbitt, E.S., Krabbenhoft, D.P., Sunderland, E.M., 2014. Global biogeochemical implications of mercury discharges from rivers and sediment burial. *Environ. Sci. Technol.* 48, 9514–9522. <https://doi.org/10.1021/es502134t>.
- Amos, H.M., Sonke, J.E., Obrist, D., Robins, N., Hagan, N., Horowitz, H.M., Mason, R.P., Witt, M., Hedgecock, I.M., Corbitt, E.S., Sunderland, E.M., 2015. Observational and modeling constraints on global anthropogenic enrichment of mercury. *Environ. Sci. Technol.* 49, 4036–4047. <https://doi.org/10.1021/es5058665>.
- Arndt, S., Jørgensen, B.B., LaRowe, D.E., Middelburg, J.J., Pancost, R.D., Regnier, P., 2013. Quantifying the degradation of organic matter in marine sediments: a review and synthesis. *Earth-Science Rev.* 123, 53–86. <https://doi.org/10.1016/j.earscirev.2013.02.008>.
- ARPAV, 2007. *Bilanci Ambientali delle aziende di Porto Marghera 1998–2007*.
- Balcom, P.H., Schartup, A.T., Mason, R.P., Chen, C.Y., 2015. Sources of water column methylmercury across multiple estuaries in the northeast U.S. *Mar. Chem.* 177, 721–730. <https://doi.org/10.1016/j.marchem.2015.10.012>.
- Bellucci, L.G., Frignani, M., Paolucci, D., Ravanelli, M., 2002. Distribution of heavy metals in sediments of the Venice Lagoon: the role of the industrial area. *Sci. Total Environ.* 295, 35–49.
- Bendoricchio, G., Di Luzio, M., Baschieri, P., Capodaglio, A.G., 1993. Diffuse pollution in the Lagoon of Venice. *Water Sci. Technol.* 28, 69–78. <https://doi.org/10.2166/wst.1993.0405>.
- Berdowski, J., Most, P., Van Der, Veldt, C., Bloos, J.P., Pacyna, J.M., Rentz, O., Oertel, D., Karl, U., Pulles, T., Appelman, W., Dellaert, S., 2017. *Manufacture of Basic Precious and Non-ferrous Metals*. EMEP/EEA, European Environment Agency.
- Bernardello, M., Secco, T., Pellizzato, F., Chinellato, M., Sfriso, A., Pavoni, B., 2006. The changing state of contamination in the Lagoon of Venice. Part 2: heavy metals. *Chemosphere* 64, 1334–1345. <https://doi.org/10.1016/j.chemosphere.2005.12.033>.
- Bettiol, C., Collavini, F., Guerzoni, S., Molinaroli, E., Rossini, P., Zaggia, L., Zonta, R., 2005. Relative contribution of atmospheric and riverine inputs of metals, nutrients and POPs into the Lagoon of Venice. *Hydrobiologia* 550, 151–165.
- Black, F.J., Poulin, B.A., Flegal, A.R., 2012. Factors controlling the abiotic photo-degradation of monomethylmercury in surface waters. *Geochim. Cosmochim. Acta* 84, 492–507. <https://doi.org/10.1016/j.gca.2012.01.019>.
- Bloom, N.S., Moretto, L.M., Scopece, P., Ugo, P., 2004. Seasonal cycling of mercury and monomethyl mercury in the Venice Lagoon (Italy). *Mar. Chem.* 91, 85–99. <https://doi.org/10.1016/j.marchem.2004.06.002>.
- Bravo, A.G., Bouchet, S., Tolu, J., Björn, E., Mateos-Rivera, A., Bertilsson, S., 2017. Molecular composition of organic matter controls methylmercury formation in boreal lakes. *Nat. Commun.* 8, 1–9. <https://doi.org/10.1038/ncomms14255>.
- Brinkmann, T., Giner Santonja, G., Schorcht, F., Roudier, S., Delgado Sancho, L., 2014. Best Available Techniques Reference Document for the Production of Chlor-alkali. <https://doi.org/10.2791/13138>.
- Canu, D., Rosati, G., 2017. Long-term scenarios of mercury budgeting and exports for a Mediterranean hot spot (Marano-Grado lagoon, Adriatic Sea). *Estuar. Coast. Shelf Sci.* 198, 518–528. <https://doi.org/10.1016/j.ecss.2016.12.005>.
- Chen, L., Zhang, W., Zhang, Y., Tong, Y., Liu, M., Wang, H., Xie, H., Wang, X., 2018. Historical and future trends in global source-receptor relationships of mercury. *Sci. Total Environ.* 610–611, 24–31. <https://doi.org/10.1016/j.scitotenv.2017.07.182>.
- Colette, A., Aas, W., Banin, L., Braban, C.F., Ferm, M., González Ortiz, A., Ilyin, I., Mar, K., Pandolfi, M., Putaud, J.-P., Shatalov, V., Solberg, S., Spindler, G., Tarasova, O., Vana, M., Adani, M., Almodovar, P., Berton, E., Bessagnet, B., Bohlin-Nizzetto, P., Boruvkova, J., Breivik, K., Briganti, G., Cappelletti, A., Cuvelier, K., Derwent, R., D'Isidoro, M., Fagerli, H., Funk, C., Garcia Vivanco, M., González Ortiz, A., Haeuber, R., Hueglin, C., Jenkins, S., Kerr, J., de Leeuw, F., Lynch, J., Manders, A., Mircea, M., Pay, M.T., Pritula, D., Putaud, J.-P., Querol, X., Raffort, V., Reiss, I., Roustan, Y., Sauvage, S., Scavo, K., Simpson, D., R.L.S., Tang, Y.S., Theobald, M., Tørseth, K., Tsyro, S., van Pul, A., Vidic, S., Wallasch, M., Wind, P., 2016. *Air Pollution Trends in the EMEP Region Between 1990 and 2012 EMEP/CCC-Report 1/2016; Joint Report of: EMEP Task Force on Measurements and Modelling (TFMM), Chemical Coordinating Centre (CCC), Meteorological Synthesizing Centre-East (MSC-E), Meteorologi*.
- Collavini, F., Bettiol, C., Zaggia, L., Zonta, R., 2005. Pollutant loads from the drainage basin to the Venice Lagoon (Italy). *Environ. Int.* 31, 939–947. <https://doi.org/10.1016/j.envint.2005.05.003>.
- Cossa, D., Harmelin-Vivien, M., Mellon-Duval, C., Loizeau, V., Averty, B., Crochet, S., Chou, L., Cadiou, J.-F., 2012. Influences of bioavailability, trophic position, and growth on methylmercury in hakes (*Merluccius merluccius*) from northwestern Mediterranean and northeastern Atlantic. *Environ. Sci. Technol.* 46, 4885–4893. <https://doi.org/10.1021/es204269w>.
- Cossa, D., Durrieu de Madron, X., Schäfer, J., Lancelleur, L., Guéron, S., Buscail, R., Thomas, B., Castelle, S., Naudin, J.-J., 2017. The open sea as the main source of methylmercury in the water column of the Gulf of Lions (northwestern Mediterranean margin). *Geochim. Cosmochim. Acta* 199, 222–237. <https://doi.org/10.1016/j.gca.2016.11.037>.
- Critto, A., Marcomini, A., 2001. *Ecological Risk and Chemical Pollution in Lagoon Environment (In Italian) - Rischio ecologico e inquinamento chimico lagunare*. 1st ed. Libreria Editrice Cafoscara, Venice.
- Critto, A., Carlon, C., Marcomini, A., 2005. Screening ecological risk assessment for the benthic community in the Venice Lagoon (Italy). *Environ. Int.* 31, 1094–1100. <https://doi.org/10.1016/j.envint.2005.05.046>.
- Dominik, J., Tagliapietra, D., Bravo, A.G., Sigovini, M., Spangenberg, J.E., Amouroux, D., Zonta, R., 2014. Mercury in the food chain of the Lagoon of Venice, Italy. *Mar. Pollut. Bull.* 88, 194–206. <https://doi.org/10.1016/j.marpolbul.2014.09.005>.
- Donazzolo, R., Orio, A.A., Pavoni, B., Perin, G., Industriale, C., San, C.L., 1984. Heavy metals in sediments of the Venice Lagoon. *Oceanol. Acta* 7, 25–32.
- EEA, n.d. *European Pollutant Release and Transfer Register, E-PRTR [WWW Document]*. Eur. Environ. Agency. URL <https://prtr.eea.europa.eu/#/home> (accessed 2.11.19).
- Emili, A., Acquavita, A., Koron, N., Covelli, S., Faganelli, J., Horvat, M., Žižek, S., Fajon, V., 2012. Benthic flux measurements of hg species in a northern Adriatic lagoon environment (Marano and Grado Lagoon, Italy). *Estuar. Coast. Shelf Sci.* 113, 71–84. <https://doi.org/10.1016/j.ecss.2012.05.018>.
- Fitzgerald, W.F., 2006. *Photodecomposition of Methylmercury in an Arctic Alaskan*. *Environ. Sci. Technol.* 40, 1212–1216.
- Gilmour, C., Bell, J.T., Soren, A.B., Riedel, Georgia, Riedel, Gerhardt, Kopec, A.D., Bodaly, R.A., 2018. Distribution and biogeochemical controls on net methylmercury production in Penobscot River marshes and sediment. *Sci. Total Environ.* 640–641, 555–569. <https://doi.org/10.1016/j.scitotenv.2018.05.276>.
- Guéron, S., Huguet, L., Vignati, D.A.L., Liu, B., Gimbert, F., Ferrari, B.J.D., Zonta, R., Dominik, J., 2012. Tidal cycling of mercury and methylmercury from sediments and water column in the Venice Lagoon (Italy). *Mar. Chem.* 130–131, 1–11. <https://doi.org/10.1016/j.marchem.2011.12.003>.
- Guerzoni, S., Tagliapietra, D., 2006. *Atlas of the lagoon: Venice between land and sea (in Italian) - Atlante della laguna: Venezia tra terra e mare [WWW document]*. URL <http://www.atlantedelalaguna.it/>.
- Han, S., Obraztsova, A., Pretto, P., Choe, K.-Y., Gieskes, J., Deheyn, D.D., Tebot, B.M., 2007. Biogeochemical factors affecting mercury methylation in sediments of the Venice Lagoon, Italy. *Environ. Toxicol. Chem.* 26, 655–663. <https://doi.org/10.1897/06-392R.1>.
- Harding, C., Dalziel, J., Vass, P., 2018. Bioaccumulation of methylmercury within the marine food web of the outer Bay of Fundy, Gulf of Maine. *PLoS One* 13, 1–30. <https://doi.org/10.1371/journal.pone.0197220>.
- Heyes, A., Mason, R.P., Kim, E.H., Sunderland, E., 2006. Mercury methylation in estuaries: insights from using measuring rates using stable mercury isotopes. *Mar. Chem.* 102, 134–147. <https://doi.org/10.1016/j.marchem.2005.09.018>.
- Hines, M.E., Poitras, E.N., Covelli, S., Faganelli, J., Emili, A., Žižek, S., Horvat, M., 2012. Mercury methylation and demethylation in hg-contaminated lagoon sediments (Marano and Grado Lagoon, Italy). *Estuar. Coast. Shelf Sci.* 113, 85–89. <https://doi.org/10.1016/j.ecss.2011.12.021>.

- Hollweg, T.A., Gilmour, C.C., Mason, R.P., 2009. Methylmercury production in sediments of Chesapeake Bay and the mid-Atlantic continental margin. *Mar. Chem.* 114, 86–101. <https://doi.org/10.1016/j.marchem.2009.04.004>.
- Hollweg, T.A., Gilmour, C.C., Mason, R.P., 2010. Mercury and methylmercury cycling in sediments of the mid-Atlantic continental shelf and slope. *Limnol. Oceanogr.* 55, 2703–2722. <https://doi.org/10.4319/lo.2010.55.6.2703>.
- Horowitz, H.M., Jacob, D.J., Amos, H.M., Streets, D.G., Sunderland, E.M., 2014. Historical mercury releases from commercial products: global environmental implications. *Environ. Sci. Technol.* 48, 10242–10250. <https://doi.org/10.1021/es501337j>.
- Joint Research Center of the European Commission, 2001. Integrated Pollution Prevention and Control (IPPC). Reference Document on Best Available Techniques in the Chlor-alkali Manufacturing Industry. Seville, Spain. <https://doi.org/10.2791/13138>.
- Kim, M., Han, S., Gieskes, J., Deheyn, D.D., 2011. Importance of organic matter lability for monomethylmercury production in sulfate-rich marine sediments. *Sci. Total Environ.* 409, 778–784. <https://doi.org/10.1016/j.scitotenv.2010.10.050>.
- Kocman, D., Horvat, M., Pirrone, N., Cinnirella, S., 2013. Contribution of contaminated sites to the global mercury budget. *Environ. Res.* 125, 160–170. <https://doi.org/10.1016/j.envres.2012.12.011>.
- Kotnik, J., Horvat, M., Ogrinc, N., Fajon, V., Žagar, D., Cossa, D., Sprovieri, F., Pirrone, N., 2015. Mercury speciation in the Adriatic Sea. *Mar. Pollut. Bull.* 96, 136–148. <https://doi.org/10.1016/j.marpolbul.2015.05.037>.
- Lamborg, C.H., Hammerschmidt, C.R., Bowman, K.L., 2016. An examination of the role of particles in oceanic mercury cycling. *Philos. Trans. R. Soc. A Math. Phys. Eng. Sci.* 374, 20150297. <https://doi.org/10.1098/rsta.2015.0297>.
- Lehnher, I., St. Louis, V.L., Hintelmann, H., Kirk, J.L., 2011. Methylation of inorganic mercury in polar marine waters. *Nat. Geosci.* 4, 298–302. <https://doi.org/10.1038/ngeo1134>.
- Marchi, T., Visentin, L., Gregio, M., Mazzuia, L., Magarotto, G., 2013. Occupational exposure to mercury during the demolition of the chlorine-soda plant in the industrial area of Venice - Esposizione professionale a mercurio durante la demolizione dell'impianto Cloro-Soda del Petrochimico di Marghera. *Ital. J. Occup. Environ. Hyg.* 4, 69–75.
- Marnane, I., Kuenen, J., Hendriks Carljin Visschedijk, A., Smit, T., Vermeulen, J., Grandjean, P., Hagström, P., Kalvig, P., Fold, N., Jönsson, J.B., Kirk, L.E., Schoeters, G., Nørgaard, S., Pirrone, N., Staff from, E.C., N.E., 2018. Mercury in Europe's Environment A Priority for European and Global Action - 1977-8449. EEA Report no 11/2018. <https://doi.org/10.2800/558803>.
- Masiol, M., Facca, C., Visin, F., Sfriso, A., Pavoni, B., 2014. Interannual heavy element and nutrient concentration trends in the top sediments of Venice Lagoon (Italy). *Mar. Pollut. Bull.* 89, 49–58. <https://doi.org/10.1016/j.marpolbul.2014.10.036>.
- Mason, R.P., Choi, A.L., Fitzgerald, W.F., Hammerschmidt, C.R., Lamborg, C.H., Soerensen, A.L., Sunderland, E.M., 2012. Mercury biogeochemical cycling in the ocean and policy implications. *Environ. Res.* 119, 101–117. <https://doi.org/10.1016/j.envres.2012.03.013>.
- Matteucci, G., Rossini, P., Guerzoni, S., Arcangeli, A., Fonti, P., Langone, L., Miserocchi, S., 2005. Recent evolution of sedimentary heavy metals in a coastal lagoon contaminated by industrial wastewaters (Pialassa Baiona, Ravenna, Italy). *Hydrobiologia* 550, 167–173. <https://doi.org/10.1007/s10750-005-4374-0>.
- MAV-CORILA, 2011. Biodisponibilità e biotossicità Dei Contaminanti Lagunari Ed Evoluzione Normativa. Rapporto Finale CORILA - Bioavailability and Toxicity of Pollutants in the Venice Lagoon, and Regulatory Changes (in Italian).
- MAV-CVN, 1999. Mappatura dell'inquinamento dei fondali lagunari. Report Finale - Mapping of Pollution of the Lagoon Sediment. Final Report (in Italian).
- MAV-CVN, 2004. Attività di monitoraggio ambientale della laguna di Venezia. Esecutivo del I stralcio triennale (2000–2003) - Environmental monitoring in the Venice Lagoon. Triennial Report (2000–2003) (in Italian).
- MAV-CVN, 2005. Attività di monitoraggio ambientale della laguna di Venezia. Esecutivo del II stralcio triennale (2002–2005) - Environmental monitoring in the Venice Lagoon. Triennial Report (2002–2005) (in Italian).
- Melaku Canu, D., Rosati, G., Solidoro, C., Heimbürger, L.-E., Acquavita, A., 2015. A comprehensive assessment of the mercury budget in the Marano-Grado Lagoon (Adriatic Sea) using a combined observational modeling approach. *Mar. Chem.* 177, 742–752. <https://doi.org/10.1016/j.marchem.2015.10.013>.
- Melaku Canu, D., Campostrini, P., Dalla Riva, S., Pastres, R., Pizzo, L., Rossetto, L., Solidoro, C., 2011. Addressing sustainability of clam farming in the Venice Lagoon. *Ecol. Soc.* 16 (3).
- Ministero dell'Ambiente e della Tutela del Territorio e del Mare, 2007. Integrated Environmental Authorization - Parere Istruttorio Conclusivo - Syndial (CS23-25) - Marghera (VE).
- Molinari, E., Sarretta, A., de Souza Guimarães, Jorge A., Botter, M., Cassin, D., Guerzoni, S., 2013. Relationship of morpho-sedimentological variations to the fate of Hg- and Zn-polluted sediments in the contaminated site of Porto Marghera, Lagoon of J. *Environ. Prot. (Irvine, Calif.)* 4, 37–49. <https://doi.org/10.4236/jep.2013.44A006>.
- Monperrus, M., Tessier, E., Amouroux, D., Leynaert, A., Huonnic, P., Donard, O.F.X., 2007a. Mercury methylation, demethylation and reduction rates in coastal and marine surface waters of the Mediterranean Sea. *Mar. Chem.* 107, 49–63. <https://doi.org/10.1016/j.marchem.2007.01.018>.
- Monperrus, M., Tessier, E., Point, D., Vidimova, K., Amouroux, D., Guyoneaud, R., Leynaert, A., Grall, J., Chauvaud, L., Thouzeau, G., Donard, O.F.X., 2007b. The biogeochemistry of mercury at the sediment-water interface in the Thau Lagoon. 2. Evaluation of mercury methylation potential in both surface sediment and the water column. *Estuar. Coast. Shelf Sci.* 72, 485–496. <https://doi.org/10.1016/j.ecss.2006.11.014>.
- Muresan, B., Cossa, D., D., J., Prévot, F., Kerbellec, S., 2007. The biogeochemistry of mercury at the sediment-water interface in the Thau lagoon. 1. Partition and speciation. *Estuar. Coast. Shelf Sci.* 72, 472–484. <https://doi.org/10.1016/j.ecss.2006.11.015>.
- Pastres, R., Solidoro, C., Cossarini, G., Canu, D.M., Dejak, C., 2011. Managing the rearing of *Tapes philippinarum* in the lagoon of Venice: a decision support system. *Ecol. Model.* 138 (1–3), 231–241.
- Pavoni, B., Donazzolo, R., Marcomini, A., Degobbis, D., Orto, A.A., 1987. Historical development of the Venice lagoon contamination as recorded in radiodated sediment cores. *Mar. Pollut. Bull.* 18, 18–24. [https://doi.org/10.1016/0025-326X\(87\)90651-5](https://doi.org/10.1016/0025-326X(87)90651-5).
- Perugini, M., 2014. Il farsi di una grande impresa. La Montecatini fra le due guerre mondiali - The Creation of a Large Corporation. The Montecatini Group Between the Two Wars. (in Italian). I. ed. Franco Angeli s.r.l, Milano, Italy.
- Porchia, F., 2012. L'evoluzione del porto industriale di Marghera dalle origini al secondo dopoguerra (1917–1963) - Historical Evolution of Marghera Industrial Harbor, From the Origins to the Second Post-war Period (1917–1963) (in Italian). PhD thesis. Univ. of Padua.
- Qureshi, A., O'Driscoll, N.J., Macleod, M., Neuhold, Y.M., Hungerbühler, K., 2010. Photoreactions of mercury in surface ocean water: gross reaction kinetics and possible pathways. *Environ. Sci. Technol.* 44, 644–649. <https://doi.org/10.1021/es9012728>.
- Rajar, R., Žagar, D., Širca, A., Horvat, M., 2000. Three-dimensional modelling of mercury cycling in the Gulf of Trieste. *Sci. Total Environ.* 260, 109–123. [https://doi.org/10.1016/S0048-9697\(00\)00555-6](https://doi.org/10.1016/S0048-9697(00)00555-6).
- Rajar, R., Četina, M., Horvat, M., Žagar, D., 2007. Mass balance of mercury in the Mediterranean Sea. *Mar. Chem.* 107, 89–102. <https://doi.org/10.1016/j.marchem.2006.10.001>.
- Ravera, O., 2000. The Lagoon of Venice: the results of both natural factors and human influence. *J. Limnol.* 59, 19–30 (doi:jlimnol.2000.19).
- Rosati, G., Heimbürger, L.E., Melaku Canu, D., Lagane, C., Laffont, L., Rijkenberg, M.J.A., Gerringa, L.J.A., Solidoro, C., Gencarelli, C.N., Hedgcock, I.M., De Baar, H.J.W., Sonke, J.E., 2018. Mercury in the Black Sea: new insights from measurements and numerical modeling. *Glob. Biogeochem. Cycles* 32, 1–22. <https://doi.org/10.1002/2017GB005700>.
- Rossini, P., Guerzoni, S., Molinaroli, E., Rampazzo, G., De Lazzari, A., Zancanaro, A., 2005. Atmospheric bulk deposition to the lagoon of Venice: part I. Fluxes of metals, nutrients and organic contaminants. *Environ. Int.* 31, 959–974. <https://doi.org/10.1016/j.envint.2005.05.006>.
- Rudd, J.W.M., Bodaly, R.A., Fisher, N.S., Kelly, C.A., Kopec, D., Whipple, C., 2018. Fifty years after its discharge, methylation of legacy mercury trapped in the Penobscot Estuary sustains high mercury in biota. *Sci. Total Environ.* 642, 1340–1352. <https://doi.org/10.1016/j.scitotenv.2018.06.060>.
- Salvagio Manta, D., Bonsignore, M., Oliveri, E., Barra, M., Tranchida, G., Giaramita, L., Mazzola, S., Sprovieri, M., 2016. Fluxes and the mass balance of mercury in Augusta Bay (Sicily, southern Italy). *Estuar. Coast. Shelf Sci.* 181, 134–143. <https://doi.org/10.1016/j.ecss.2016.08.013>.
- Santschi, P.H., Yeager, K.M., Schwehr, K.A., Schindler, K.J., 2017. Estimates of recovery of the Penobscot River and estuarine system from mercury contamination in the 1960's. *Sci. Total Environ.* 596–597, 351–359. <https://doi.org/10.1016/j.scitotenv.2017.04.094>.
- Sarretta, A., Pilon, S., Molinaroli, E., Guerzoni, S., Fontolan, G., 2010. Sediment budget in the Lagoon of Venice, Italy. *Cont. Shelf Res.* 30, 934–949. <https://doi.org/10.1016/j.csr.2009.07.002>.
- Schartup, A., Thackray, C., Qureshi, A., Dassuncao, C., Gillespie, K., Hanke, A., Sunderland, E., 2019. Climate change and overfishing increase neurotoxicant in marine predators. *Nature* 572, 1–3. <https://doi.org/10.1038/s41586-019-1468-9>.
- Schartup, A.T., Balcom, P.H., Soerensen, A.L., Gosnell, K.J., Calder, R.S.D., Mason, R.P., Sunderland, E.M., 2015a. Freshwater discharges drive high levels of methylmercury in Arctic marine biota. *Proc. Natl. Acad. Sci.* 112, 11789–11794. <https://doi.org/10.1073/pnas.1505541112>.
- Schartup, A.T., Ndu, U., Balcom, P.H., Mason, R.P., Sunderland, E.M., 2015b. Contrasting effects of marine and terrestrially derived dissolved organic matter on mercury speciation and bioavailability in seawater. *Environ. Sci. Technol.* 49, 5965–5972. <https://doi.org/10.1021/es506274x>.
- Selin, H., Keane, S.E., Wang, S., Selin, N.E., Davis, K., Bally, D., 2018. Linking science and policy to support the implementation of the Minamata convention on mercury. *Ambio* 47, 198–215. <https://doi.org/10.1007/s13280-017-1003-x>.
- Sfriso, A., Facca, C., Marcomini, A., 2005. Sedimentation rates and erosion processes in the lagoon of Venice. *Environ. Int.* 31, 983–992. <https://doi.org/10.1016/j.envint.2005.05.008>.
- Sfriso, A.A., Sfriso, A., 2017. In situ biomass production of Gracilariaceae and *Ulva rigida*: the Venice Lagoon as a study case. *Bot. Mar.* 60, 271–283. <https://doi.org/10.1515/bot-2016-0061>.
- Sharif, A., Monperrus, M., Tessier, E., Bouchet, S., Pinaly, H., Rodriguez-Gonzalez, P., Maron, P., Amouroux, D., 2014. Fate of mercury species in the coastal plume of the Adour River estuary (Bay of Biscay, SW France). *Sci. Total Environ.* 496, 701–713. <https://doi.org/10.1016/j.scitotenv.2014.06.116>.
- Soerensen, A.L., Schartup, A.T., Gustafsson, E., Gustafsson, B.G., Undeman, E., Björn, E., 2016. Eutrophication increases phytoplankton methylmercury concentrations in a coastal sea—a Baltic sea case study. *Environ. Sci. Technol.* 50, 11787–11796. <https://doi.org/10.1021/acs.est.6b02717>.
- Soerensen, A.L., Schartup, A.T., Skrobonja, A., Björn, E., 2017. Organic matter drives high interannual variability in methylmercury concentrations in a subarctic coastal sea. *Environ. Pollut.* 229, 531–538. <https://doi.org/10.1016/j.envpol.2017.06.008>.
- Solidoro, C., Brando, V.E., Dejak, C., Franco, D., Pastres, R., Pecenic, G., 1997a. Long term simulations of population dynamics of *Ulva r.* in the lagoon of Venice. *Ecol. Model.* 102 (2–3), 259–272.
- Solidoro, C., Pecenic, G., Pastres, R., Franco, D., Dejak, C., 1997b. Modelling macroalgae (*Ulva rigida*) in the Venice lagoon: model structure identification and first parameters estimation. *Ecol. Model.* 94 (2), 191–206.

- Solidoro, C., Pastres, R., Melaku Canu, D., Pellizzato, M., Rossi, R., 2000. Modelling the growth of *Tapes philippinarum* in northern Adriatic lagoons. *Mar. Ecol. Prog. Ser.* 199, 137–148. <https://doi.org/10.3354/meps199137>.
- Solidoro, C., Melaku Canu, D., Cucco, A., Umgiesser, G., 2004. A partition of the Venice lagoon based on physical properties and analysis of general circulation. *J. Mar. Syst.* 51, 147–160. <https://doi.org/10.1016/j.jmarsys.2004.05.010>.
- Solidoro, C., Pastres, R., Cossarini, G., 2005. Nitrogen and plankton dynamics in the lagoon of Venice. *Ecol. Model.* 184, 103–123. <https://doi.org/10.1016/j.ecolmodel.2004.11.009>.
- Solidoro, C., Bandelj, V., Bernardi, F.A., Camatti, E., Ciavatta, S., Cossarini, G., Facca, C., Franzoi, P., Libralato, S., Canu, D.M., Pastres, R., Pranovi, F., Raicevich, S., Socal, G., Sfriso, A., Sigovini, M., Tagliapietra, D., Torricelli, P., 2010. Response of the Venice Lagoon ecosystem to natural and anthropogenic pressures over the last 50 years. *Coastal Lagoons: Critical Habitats of Environmental Change*. Taylor & Francis Group, pp. 483–511 <https://doi.org/10.1201/EBK1420088304-c19>.
- Sommerfreund, J.K., Gandhi, N., Diamond, M.L., Mugnai, C., Frignani, M., Capodaglio, G., Gerino, M., Bellucci, L.G., Giuliani, S., 2010. Contaminant fate and transport in the Venice Lagoon: results from a multi-segment multimedia model. *Ecotoxicol. Environ. Saf.* 73, 222–230. <https://doi.org/10.1016/j.ecoenv.2009.11.005>.
- Storelli, M.M., Barone, G., 2013. Toxic metals (Hg, Pb, and Cd) in commercially important Demersal fish from Mediterranean Sea: contamination levels and dietary exposure assessment. *J. Food Sci.* 78, T362–T366. <https://doi.org/10.1111/j.1750-3841.2012.02976.x>.
- Streets, D.G., Devane, M.K., Lu, Z., Bond, T.C., Sunderland, E.M., Jacob, D.J., 2011. All-time releases of mercury to the atmosphere from human activities. *Environ. Sci. Technol.* 45, 10485–10491. <https://doi.org/10.1021/es202765m.ALL-TIME>.
- Streets, D.G., Horowitz, H.M., Jacob, D.J., Lu, Z., Levin, L., ter Schure, A.F.H., Sunderland, E.M., 2017. Total mercury released to the environment by human activities. *Environ. Sci. Technol.* 51, 5969–5977. <https://doi.org/10.1021/acs.est.7b00451>.
- Streets, D.G., Horowitz, H.M., Lu, Z., Levin, L., Thackray, C.P., Sunderland, E.M., 2019. Global and regional trends in mercury emissions and concentrations, 2010–2015. *Atmos. Environ.* 201, 417–427. <https://doi.org/10.1016/j.atmosenv.2018.12.031>.
- Sunderland, E.M., Selin, N.E., 2013. Future trends in environmental mercury concentrations: implications for prevention strategies. *Environ. Health* 12, 1–5. <https://doi.org/10.1186/1476-069X-12-2>.
- Sunderland, E.M., Gobas, F.A.P.C., Branfireun, B.A., Heyes, A., 2006. Environmental controls on the speciation and distribution of mercury in coastal sediments. *Mar. Chem.* 102, 111–123. <https://doi.org/10.1016/j.marchem.2005.09.019>.
- Turner, R.R., Kopec, A.D., Charette, M.A., Henderson, P.B., 2018. Current and historical rates of input of mercury to the Penobscot River, Maine, from a chlor-alkali plant. *Sci. Total Environ.* 637–638, 1175–1186. <https://doi.org/10.1016/j.scitotenv.2018.05.090>.
- Umgiesser, G., Melaku Canu, D., Solidoro, C., Ambrose, R., 2003. A finite element ecological model: a first application to the Venice Lagoon. *Environ. Model. Softw.* 18, 131–145. [https://doi.org/10.1016/S1364-8152\(02\)00056-7](https://doi.org/10.1016/S1364-8152(02)00056-7).
- Umgiesser, G., Canu, D.M., Cucco, A., Solidoro, C., 2004. A finite element model for the Venice Lagoon. Development, set up, calibration and validation. *J. Mar. Syst.* 51, 123–145. <https://doi.org/10.1016/j.jmarsys.2004.05.009>.
- Wool, T.A., Ambrose, R.B., Martin, J.L., Comer, E.A., 2001. *Water Quality Analysis Simulation Program (WASP) Version 6.0: User's Manual*.
- Žagar, D., Knap, A., Warwick, J.J., Rajar, R., Horvat, M., Cetina, M., 2006. Modelling of mercury transport and transformation processes in the Idrijca and Soca river system. *Sci. Total Environ.* 368, 149–163. <https://doi.org/10.1016/j.scitotenv.2005.09.068>.
- Zonta, R., Botter, M., Cassin, D., Bellucci, L.G., Pini, R., Dominik, J., 2018. Sediment texture and metal contamination in the Venice lagoon (Italy): A snapshot before the installation of the MOSE system. *Estuar. Coast. Shelf Sci.* 205, 131–151. <https://doi.org/10.1016/j.ecss.2018.03.007>.
- Zuliani, A., Zaggia, L., Collavini, F., Zonta, R., 2005. Freshwater discharge from the drainage basin to the Venice Lagoon (Italy). *Environ. Int.* 31, 929–938. <https://doi.org/10.1016/j.envint.2005.05.004>.